CHAPTER 3

Laser Resonators with Brillouin Mirrors

MARTIN OSTERMEYER and RALF MENZEL
University of Potsdam, Institute of Physics, Chair of Photonics, 14469 Potsdam, Germany

3.1 INTRODUCTION

As has been shown in the preceding chapter, nonlinear mirrors based on stimulated Brillouin scattering (SBS mirrors) can be used to produce the phase conjugate of a wavefront [1, 2] with a fidelity close to one. There are two major different ways of realizing high-power lasers with excellent beam quality (high-brightness lasers). One is the laser oscillator, and the second is the master oscillator power amplifier concept (MOPA). Depending on the specific application, either the laser oscillator or the MOPA concept might be more appropriate. Phase conjugating SBS mirrors can be applied in both designs to compensate for phase distortions in the laser-active medium. Especially in solid-state lasers where the thermal load due to the pump is a serious problem, these concepts to improve the beam quality can be useful. The phase conjugating SBS mirror is easy to use since it is self-pumped by the incident beam. However, if SBS-phase conjugation is applied inside a laser resonator, a more elaborate Brillouin-enhanced four-wave mixing (BEFWM) scheme is the appropriate description of the physical process. As a consequence, the threshold of bulk SBS mirrors is decreased if they are placed in a resonator.

The motivation to use a phase conjugating mirror (PCM) within a laser resonator or simply to replace one of the resonator mirrors by the PCM is at least twofold. Besides the compensation of phase distortions to achieve an excellent beam quality, also the stability of phase conjugate resonators (PCR) is guaranteed and independent from the specific resonator design (see Section 3.3). Thus, fluctuating or drifting optical parameters in the laser resonator such as a fluctuating thermal lens in a solid-state laser can be dynamically corrected in a properly designed PCR. As a result, the beam parameters of the solid-state laser will be independent of the pump power. A further consequence is that the misalignment sensitivity of the resonator is reduced.

If the PCM is based on SBS apart from these two complexes known as aberration compensation and resonator stability, there are other motives arising to use such an

Phase Conjugate Laser Optics, edited by Arnaud Brignon and Jean-Pierre Huignard
ISBN 0-471-43957-6

SBS mirror in addition. For instance, the frequency shifting effect of the SBS mirror can be used to generate a large bandwidth and short pulses in injected resonators [3, 4] (see Section 3.6.1) or it can be used to avoid gain competition for counter-propagating waves in the laser-active material [5, 6] (see Section 3.2). The nonlinear properties of the SBS mirror inside the resonator (see previous chapter) give the opportunity for two major applications. One is *Q*-switching the laser resonator (see Section 3.4). Secondly, amplified spontaneous emission (ASE) can be avoided, for example, in regenerative amplifiers [7–13], but regenerative amplifiers are not dealt with here. To decrease the threshold of bulk SBS mirrors, they were placed in resonators just by themselves. Again for these techniques the reader is referred to the original literature [14–18].

Different laser resonator schemes containing SBS mirrors (SBS-laser oscillators) have been demonstrated and presented in the literature. An overview of the different types will be given in Section 3.2. The most prominent of the SBS-laser oscillators is probably also the most straightforward realization of a linear SBS-laser oscillator (sf-SBS laser). The description of this kind will take most of the space of this chapter. Section 3.3 deals with the transverse eigensolutions in SBS-PCRs.

The passive *Q*-switch of the SBS-laser oscillator is described in detail, and the variation of the pulse energy is explained and calculated from the properties of the start resonator in Section 3.4. It turns out that gaseous SBS mirrors are very efficient *Q*-switch devices for laser oscillators with a high gain factor and high average output power. *Q*-switched lasers with an SBS cell can reach even slightly higher efficiencies than comparable free running lasers as will be shown in Section 3.7.

Inside a laser resonator the SBS threshold can be reduced by a resonant generation of the sound wave [19, 20] from the longitudinal laser modes. It will be shown in Section 3.5 that the resonance condition for the so-called start resonator is a key precondition for reliable operation of a laser oscillator with phase conjugating SBS mirror.

The reflection at the moving sound wave in the SBS mirror leads to a Doppler shift (Brillouin shift) of the backscattered light. This causes a transient longitudinal mode spectrum of the SBS laser as will be shown in Section 3.6.

There are other possibilities than SBS to realize a phase conjugating cavity mirror. In the 1970s and 1980s, four-wave mixing and BEFWM were more in the focus to realize phase conjugating laser mirrors (see, e.g., Refs. 21–23). These techniques lead to PCMs without a threshold behavior. But high-quality pump beams are required to realize such a PCM. Photorefractive cavity mirrors are discussed in Chapter 9 of this book, gain gratings in Chapter 10 and other techniques in Chapters 10 and 11.

3.2 SURVEY OF DIFFERENT RESONATOR CONCEPTS WITH BRILLOUIN MIRRORS

The first laser resonator with an SBS mirror was realized in 1967 by Pohl [24]. This was even before experimental and theoretical evidence was found that SBS can be

used for optical phase conjugation. Consequently, Pohl talks about a new *Q*-switching technique "only" and does not claim anything about a phase conjugate resonator or mirror.

This section gives a survey of different SBS-laser resonator concepts. Crucial points for the design of these resonators with emphasis on high average power operation specifically in the sf-SBS laser are addressed later in more detail in Section 3.7.

Due to the SBS threshold behavior, all the laser oscillators presented here are pulsed lasers, and almost all reported SBS-laser resonator designs initiate the laser process in a start resonator built by two conventional mirrors. The benefits or necessity of this will become clearer in Sections 3.4 to 3.6.3.

To our knowledge, there are only three SBS lasers reported which operate without a starter cavity. Jingguo and Hongwei [25] replaced the high reflectivity resonator mirror with a stimulated Rayleigh scattering mirror. The laser starts to "oscillate" as a super-radiator aided by the output coupling mirror only. With high pump rates they obtained emitted light to initiate the stimulated scattering process. In this case the gain of the stimulated Rayleigh scattering was greatly enhanced by absorption of light in the medium. Thus, this method is not suitable to realize lasers with high average output powers. The second laser of this kind was one of the lasers Pohl reported in Ref. 24. In his setup the SBS mirror acted as an output coupler. Also, Eichler et al. [26] reported on an excimer laser where a generator amplifier arrangement of two SBS cells acted as the high-reflecting mirror of the laser resonator.

SBS lasers with start resonator can be realized in many different ways. Figure 3.1 contains a scheme of the straightforward realization of a linear SBS-laser oscillator (sf-SBS laser). This concept exhibits a conventional start resonator between the mirrors M1 and M_{start}. M_{start} has a merely small reflectivity R_{start}. The telescope consisting of the lenses L1 and L2 reduces the coherence demands on the laser light for the SBS process (see Section 3.7).

The laser operates in the following way: At the beginning of optical pumping, there is no light power in the resonator, and the SBS mirror is transparent due to its threshold behavior. The laser starts to oscillate in the start resonator. While the intracavity power is increasing, the SBS-threshold power is reached at some time

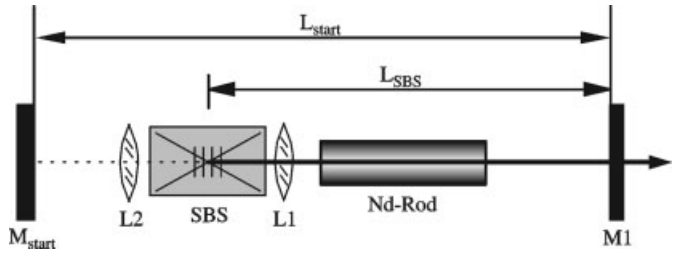

Figure 3.1. Scheme of the linear straightforward SBS-laser oscillator (sf-SBS laser).

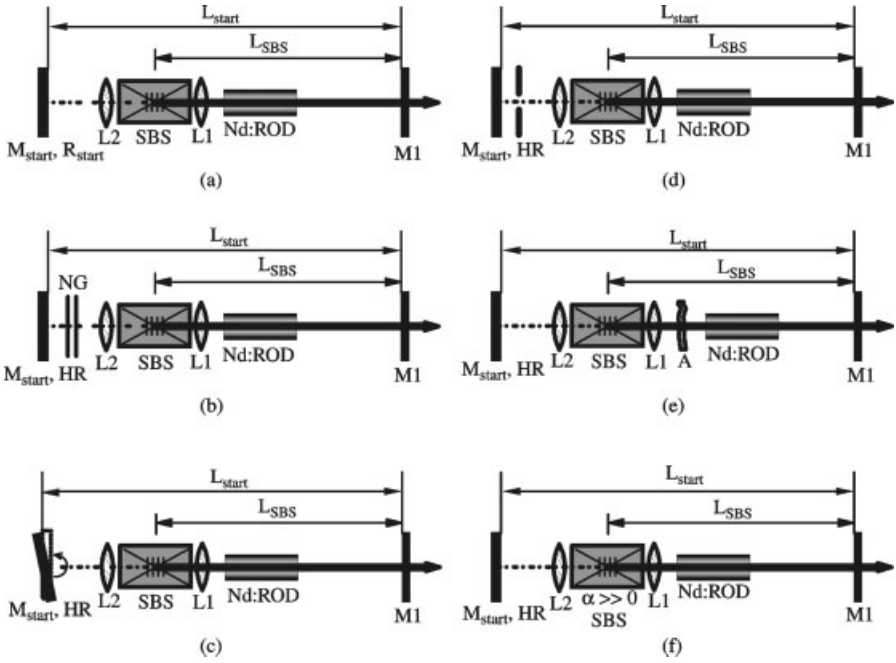

Figure 3.2. Concepts to realize a *Q*-difference between the start and the SBS resonator.

and then the reflectivity of the SBS mirror increases rapidly. Finally, the start resonator mirror M_{start} is nearly "switched off" and a giant pulse is emitted out of the SBS resonator between the output coupling mirror M1 and the SBS mirror. A smaller reflectivity of the mirror M_{start}, R_{start}, will lead to a higher pulse energy, and a larger R_{start} will lead to a smaller pulse energy. More inversion can be built up when the start resonator gets above threshold later. If the laser is further pumped after the pulse has been emitted, further *Q*-switched pulses are generated in the same manner. This way a whole burst of *Q*-switched pulses can be generated.

In order to switch the laser oscillation from the start to the SBS resonator, a difference in the quality *Q* between the two resonators is necessary. There are different possibilities to realize this *Q* difference in the sf-SBS laser (see Fig. 3.2). One easy and frequently used option is to choose the reflectivity of M_{start} smaller than the average reflectivity of the SBS mirror above threshold. The optimum value of M_{start} can be determined by inserting neutral density filters in front of the mirror (Fig. 3.2b) [19, 20, 27–29]. Moreover, the start resonator can be set up unstable (Fig. 3.2a) [18, 30, 31], elements of the start resonator can be slightly misaligned (Fig. 3.2c) [32], or a mode-selecting aperture between SBS mirror and M_{start} can be used (Fig. 3.2d) [30]. An aberrator also will lead to a higher *Q* for the phase conjugating SBS resonator than for the start resonator (Fig. 3.2e) [33]. The case shown in Fig. 3.2e is realized in every oscillator with an aberrated refractive index profile of the active laser material. Furthermore, absorbing SBS materials like CS_2 or acetone will lead to higher losses for the full transmission of the SBS cell in start

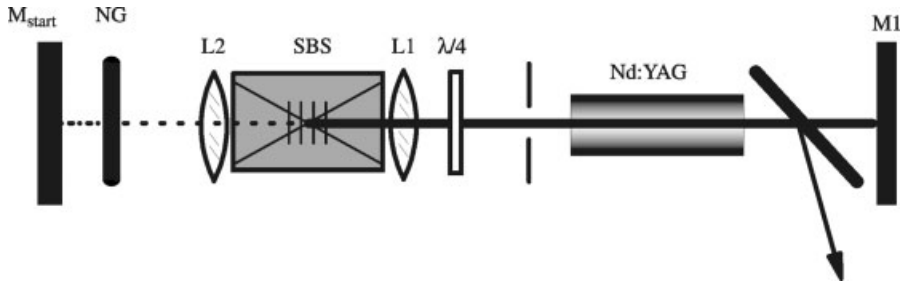

Figure 3.3. Polarization-dependent outcoupling.

resonator operation compared to the shorter path in the SBS resonator only (Fig. 3.2f) [34].

In a similar, slightly different concept the light is coupled out using a quarter-wave plate and a polarizer [35] (see Fig. 3.3). In the sf-SBS laser the output pulse energy can be varied by the reflectance of M_{start} or a filter in front of M_{start}. Here it can be done by rotating the quarter-wave plate to change the rotation angle of the intracavity field. In the first case solely the Q of the start resonator is varied. In the latter case the Qs of both the start resonator and the SBS resonator are changed.

A fundamentally different SBS-laser concept was invented by Chandra et al. [36] (see Fig. 3.4) and was later used by others also [35, 37]. Here the SBS mirror is placed outside the resonator. The concept uses the polarization status of the light to discriminate between a start and an SBS resonator. The Q ratio of the two resonators can be adjusted by rotating the quarter-wave plate. Placing the SBS-mirror extracavity makes the alignment of the focusing lens in front of the SBS mirror uncritical compared to the intracavity telescope (see above). Also, absorbing media intracavity leading to wavefront distortions or filamentation can be used with high average output powers in this scheme. On the other hand, one gives up the threshold

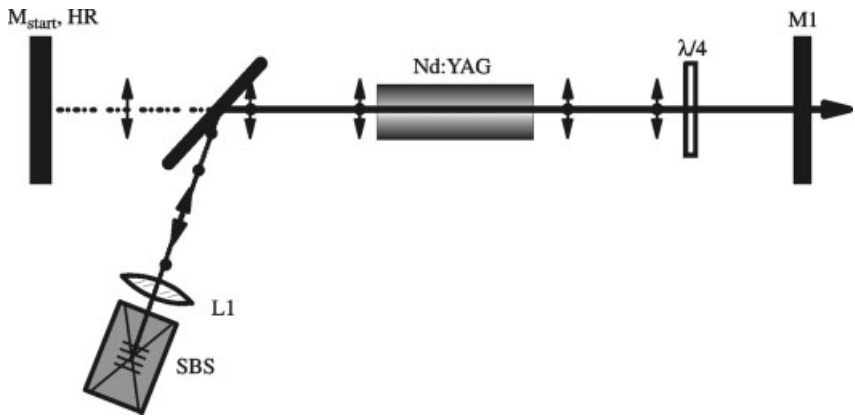

Figure 3.4. Phase conjugated resonator with sidearm SBS mirror.

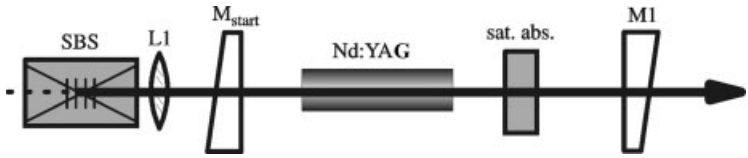

Figure 3.5. Linear, seeded SBS laser.

reduction obtained for the intracavity SBS-mirror scheme, and a larger fraction of the conventional start resonator mode is superposed to the SBS-laser mode.

Another design with the SBS mirror outside the start resonator is shown in Fig. 3.5 [38, 39]. Pashinin and Shklovsky [38] realized a start resonator confined by two uncoated wedged glass substrates. This resonator was *Q*-switched with a saturable absorber. Apparently, this was necessary to overcome the threshold of the extracavity SBS mirror. The authors claim that the mode out of the conventional start resonator had a significantly smaller mode volume than the mode with an SBS mirror in operation. Both were diffraction-limited up to repetition rates of 3 Hz.

In other schemes a second SBS mirror was used for different purposes. Typical pulse lengths of around 30 ns are too short for many applications in material processing due to plasma generation at high peak powers. In Ref. 40, Seidel and Phillipps reported on an SBS laser with two intracavity SBS cells for stretching the *Q*-switch pulses (see Fig. 3.6) . The SBS laser is based on a polarization-dependent output coupling scheme, in which the losses can be adjusted by a quarter-wave plate ($\lambda/4_{out}$) as pointed out above. The effective reflectivity of the second SBS cell can be adjusted using the two additional quarter-wave plates ($\lambda/4_{stretch1}$ and $\lambda/4_{stretch2}$ in Fig. 3.6) to out-couple radiation via the polarizer $P_{stretch}$. With this additional output coupling, the pulse duration was stretched by about a factor of 5.

In the SBS laser presented by Anikeev and Munch [13] a second extracavity SBS cell is used to extract more power out of the SBS laser and simultaneously compress the *Q*-switch pulse (see Fig. 3.7). This way the original values of 30-mJ pulse energy and 65-ns pulse duration were transformed to 65 mJ and 7 ns.

SBS mirrors in ring resonators are mostly used to feedback one of the circulating directions [10, 11, 41–43]. Therefore they are positioned outside the actual

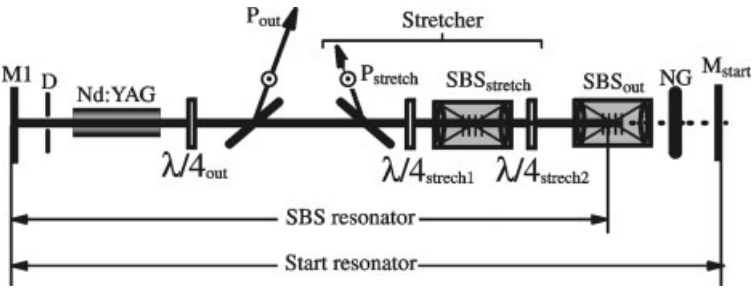

Figure 3.6. Two intracavity SBS cells to enlarge *Q*-switch pulse duration.

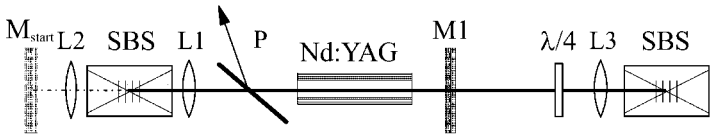

Figure 3.7. SBS laser with an additional extracavity SBS mirror to enhance extraction efficiency and compress pulses.

resonator. The ring resonator scheme presented by Lamb [6] is depicted in Fig. 3.8. It is similar to the other cited ones. It essentially represents an oscillator double-pass amplifier arrangement with one rod only. It exhibits good energy extraction due to the partial feedback of the output by the SBS mirror. *Q*-switching is initiated by the intracavity saturable absorber. The SBS cell contributes to the *Q*-switching process, and thus a shortening of the pulse duration from 22 ns to 7 ns and increasing the peak power by 32 times was observed. Since the feedback light with power P_c is frequency-shifted by the Brillouin frequency, spatial hole burning of the counterpropagating waves is prevented and stable single-frequency operation can be achieved.

Barrientos et al. [5] present a numerical investigation of an externally injected SBS ring laser. They mainly discuss the influence of the acoustic decay time of the SBS material. In Section 3.6.4 we present similar correlations for a standing-wave sf-SBS laser according to investigations of the same authors [44]. Another different ring resonator incorporating a loop like Brillouin enhanced for wave mixing mirror

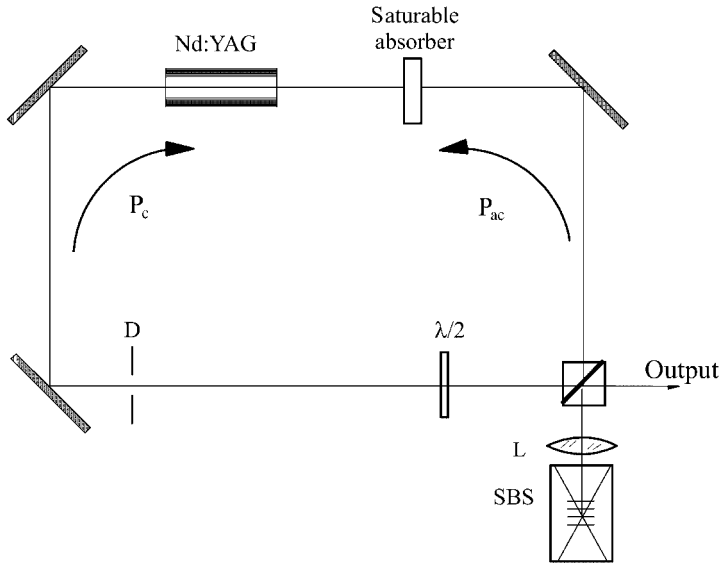

Figure 3.8. Ring laser with extracavity SBS mirror.

is reported in Ref. 45 and theoretically investigated in Ref. 46. With this scheme the subsequent frequency downshifting as it is obtained with simple SBS mirrors (see Section 3.6.1) in resonators can be avoided. Instead, in this scheme the light frequency is alternately shifted up and down.

A large number of resonator schemes with an SBS mirror to encounter certain problems of conventional resonators is known. Depending on the specific application, one of the presented schemes may be favorable. For efficient high-power Q-switch operation, the straightforward linear SBS-laser oscillator (sf-SBS laser) is probably the most simple and elegant design. It combines the advantage of a small number of resonator elements with the SBS self-Q-switching and the mechanism of threshold reduction due to the intracavity setup of the SBS mirror. When, for example, polarization and single-frequency operation become an issue, other schemes (e.g., the ring schemes) become more relevant.

3.3 STABILITY AND TRANSVERSE MODES OF PHASE CONJUGATING LASER RESONATORS WITH BRILLOUIN MIRRORS (SBS-PCRs)

A few general aspects on phase conjugating resonators (PCRs) will be discussed briefly here before we point out more precisely the theoretically predicted mode behavior in an SBS-PCR. These considerations in this section do not include an impact of any start resonator on the PCR. The phase conjugating resonator is thought to be confined by a conventional mirror (CM) as output coupler and the phase conjugating mirror (PCM). Only the term of perturbation stability, introduced in this section, allows for some consideration of the start resonator influence, however.

3.3.1 General aspects of an ideal PCR [48] For simplicity, first, we suppose an ideal PCM with the fidelity of 1, with no threshold behavior and no frequency shift. This PCM operates in a configuration as depicted in Fig. 3.9. We consider only one transverse coordinate x without restricting the general case. This propagation of the field through the phase perturbation $\rho(x)$, along with the optical

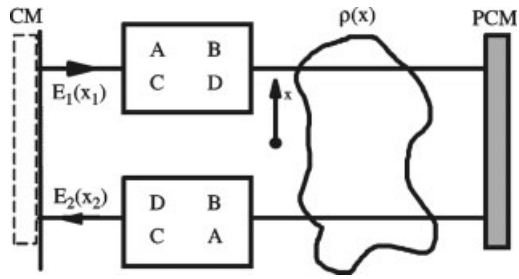

Figure 3.9. Out- and back-propagation of an arbitrary field using a phase conjugating mirror.

ABCD system to the PCM and back, can be formulated using the Collins integral:

$$E_2(x_2)=\rho(x_2)\cdot\frac{k}{2\pi|B|}\times\int_{-w_{\mathrm{PCM}}}^{w_{\mathrm{PCM}}}\left\{dx_{\mathrm{PCM}}\left[\int_{-a}^{a}dx_1\rho(x_1)E_1(x_1)\cdot\exp\left(i\frac{k}{2B}\left(Ax_1^2-2x_{\mathrm{PCM}}x_1+Dx_{\mathrm{PCM}}^2\right)\right)\right]^*\times\exp\left(-i\frac{k}{2B}\left(Dx_{\mathrm{PCM}}^2-2x_2x_{\mathrm{PCM}}+Ax_2^2\right)\right)\right\} \tag{1}$$

$2w_{\mathrm{PCM}}$ is the width of the PCM mirror; $2a$ is the width of any aperture in the reference plane.

We can absorb the width of the conventional mirror into the phase perturbation function $\rho(x)$ and extend the integration to $\pm$ infinity. If we further assume that we have real *ABCD* elements only (no transverse losses or gain variations), the integration kernel becomes more simple, and we can perform the integration at the PCM plane and write [47]

$$E_2(x_2)=\rho(x_2)\cdot\int_{-\infty}^{\infty}\rho(x_1)^*E_1^*(x_1)\cdot\exp\left(-i\frac{kA}{2B}\left(x_2^2-x_1^2\right)\right)\times\frac{\sin\left(kw_{\mathrm{PCM}}/B\right)(x_2-x_1)}{\pi(x_2-x_1)}dx_1 \tag{2}$$

In case of an unbound phase conjugate mirror, w_{PCM} becomes infinite, the $\sin(x)/x$ function acts as a Dirac-like function, and Eq. (2) simplifies to

$$E_2(x)=|\rho(x)|^2\cdot E_1^*(x) \tag{3}$$

Since $\rho(x)$ is a phase perturbation only, its square is equal to 1. Then, Eq. (3) expresses the fact that after the back-and-forth journey via a phase conjugate reflection, the phase conjugate of the initial field is yielded again. Now we can complement the whole arrangement by a conventional mirror (CM) in the reference plane to make it a PCR. Any phase shift (e.g., from a curved mirror) can be absorbed in the phase perturbation term $\rho(x)$, so that a plane conventional mirror remains. The resonator eigenvalue equation then reads

$$E_2(x)=E_1^*(x)=\gamma E_1(x) \tag{4}$$

This is fulfilled by any field distribution with a plane wavefront $E_1(x)=|E_1(x)|*\exp(i\phi)$, where ϕ is independent of x. Thus γ becomes 1 and we can conclude that any field with a wavefront matching the conventional mirror curvature is an eigensolution of a PCR. It should be noticed that this means that arbitrary phase

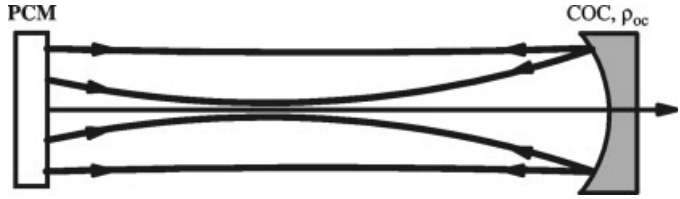

Figure 3.10. Example of double round-trip eigensolution in ideal PCR.

perturbations are perfectly compensated in an ideal unbounded PCR as it is suspected, and one of the major motivations to use PCRs is hereby justified. Furthermore, this means that the ideal PCR is always stable-independent from its specific design.

A double round trip can be treated by applying Eq. (3) two times in a row, yielding a field $E_4(x) = |\rho(x)|^4 * E_1(x)$. Again $|\rho(x)|^4$ equals 1, and therefore after two round trips any field distribution without any further condition is reproduced in such an ideal PCR (see Fig. 3.10).

3.3.2 Gaussian mode analysis of PCRs Now, we neglect any phase distortion in the resonator for a while to learn more about the lowest-order mode of an SBS-PCR and its perturbation stability. In this case, we can work with a simple *ABCD* matrix formalism and the SBS-PCRs can be treated within the complex paraxial matrix formalism.

In searching for the eigensolutions of PCRs, we have to obey special calculation rules for optical systems containing phase conjugate optics. The *ABCD* law for an optical system has to be rewritten, so that the condition for the self-consistent solution reads

$$\frac{1}{q_E} = \frac{C + (1/q_E)^* D}{A + (1/q_E)^* B} \tag{5}$$

The roundtrip in the resonator may start and end at the conventional mirror (see Fig. 3.11). Assuming a flat conventional mirror is not a restriction of the general

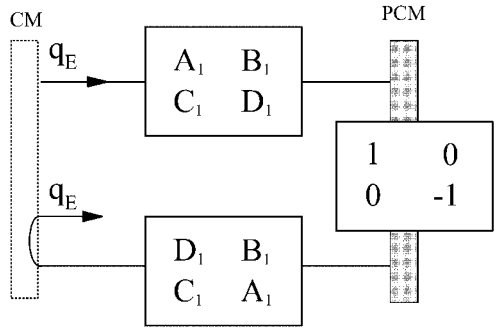

Figure 3.11. Round-trip model to calculate the eigensolutions of a general complex PCR.

case, since any curved mirror can be absorbed in two halves into the transfer matrices for the back-and-forth journey.

Taking care of the coefficient exchange of the A and D element for the back-and-forth journey the $ABCD$ matrix for the round trip reads

$$\begin{aligned} M_{\mathrm{rt}} &\equiv \begin{pmatrix} A & B \\ C & D \end{pmatrix} = M_{\mathrm{back}} M_{\mathrm{PCM}} M_{\mathrm{out}} M_{\mathrm{CM}} \\ &= \begin{pmatrix} D_1 & B_1 \\ C_1 & A_1 \end{pmatrix} \begin{pmatrix} 1 & 0 \\ 0 & -1 \end{pmatrix} \begin{pmatrix} A_1^* & B_1^* \\ C_1^* & D_1^* \end{pmatrix} \\ &= \begin{pmatrix} A_1^* D_1 - C_1^* B_1 & B_1^* D_1 - D_1^* B_1 \\ A_1^* C_1 - C_1^* C_1 & B_1^* C_1 - D_1^* A_1 \end{pmatrix} \end{aligned} \tag{6}$$

Note that the matrix for the path toward the PCM is conjugated to take the phase conjugate reflection for the complex matrix elements into account (see Chapter 1). The C and B elements are purely imaginary. In case of real matrix elements, meaning no transverse gain or aperturing profiles in the resonator, the round-trip matrix becomes the unity matrix. In this case, Eq. (5) reads $1/q_E = (1/q_E)^*$. This is consistent with the result from the last subsection. There we obtained that the single round-trip solution in an unbound PCR has no restrictions for the beam radius except to match the conventional mirror curvature that was assumed to be flat.

Introducing the purely real elements A_m, B_m, C_m, D_m,

$$\begin{aligned} A &= A_m \cdot e^{-i\theta_m} \\ B &= -iB_m \\ C &= iC_m \\ D &= -A_m^* \end{aligned} \tag{7}$$

Siegman et al. [48] showed that in the general case of *complex* matrix elements the eigensolution is discrete and the beam radius w_{CM} and wavefront curvature R_{CM} read as follows for the reference plane at the conventional mirror:

$$\begin{aligned} \frac{1}{R_{\mathrm{CM}}} &= \pm\sqrt{\frac{C_m}{B_m}} \sin\theta_m \\ \frac{\lambda}{\pi w_{\mathrm{CM}}^2} &= \pm\sqrt{\frac{C_m}{B_m}} \cos\theta_m \end{aligned} \tag{8}$$

Thus, for example, an introduction of an arbitrary weak aperture will lead to a discrete solution in the PCR. The eigensolution for the general complex PCR is discussed further in Refs. 48 and 49. We will now proceed and consider the

perturbation stability. The eigensolution for the specific example of a PCR that is a reasonable model for a real SBS-PCR is discussed later in more detail.

Apart from being confined, to be useful the transverse mode also has to be stable against perturbations. The stability of the PCR against perturbations can be tested considering a growth rate per round trip of the deviation Δq_2 from the self-consistent complex beam parameter q_E. We consider an injected mode with a complex beam parameter deviating by Δq_1 from the beam parameter q_E of the nonperturbed eigenmode of the PCR [50]. After one round trip the deviation has become Δq_2. And the growth rate results in

$$\frac{\Delta q_2}{\Delta q_1^*} = \frac{1}{(A + B \cdot (1/q_E^*))^2} \tag{9}$$

This leads to a perturbation stable mode if $|(\Delta q_2)/(\Delta q_1^*)| < 1$. Whether this inequality holds or not in the case of an SBS-PCM will be discussed below.

3.3.3 Example: SBS-PCR as PCR with soft aperture The phase conjugating SBS mirror exhibits a transverse graded reflectivity if operated below saturation of the Brillouin gain, since it is self-pumped by a transversely varying intensity. This is equivalent to a combination of an ideal PCM with a soft aperture. The aperture shall be shaped according to the incident field. It is reasonable for near-diffraction-limited beams to assume a Gaussian reflectivity distribution of the SBS mirror. The *ABCD* matrix for the SBS-PCM then becomes the product of an ideal PCM with an apodized Gaussian aperture of transmission $T(r) = T_0 \cdot \exp(-r^2/w_a^2)$, where w_a is the beam radius of the incoming Gaussian beam.

$$M_{\mathrm{SBS-PCM}} = \begin{pmatrix} 1 & 0 \\ -\dfrac{i\lambda}{\pi w_a^2} & -1 \end{pmatrix} \tag{10}$$

There are two possibilities to describe such an SBS-PCR. Giuliani et al. [51] developed a model based on a back-and-forth propagation through the resonator starting at the SBS-PCM and ending there. This interrupted round trip is closed with separate equations describing the reflectivity at the SBS mirror. Secondly, the complete uninterrupted round-trip matrix used in the self-consistency condition for a full round trip leads to the same solution. In the latter case the round-trip matrix contains the matrix for the phase conjugating mirror with radial graded reflectivity. No extra equations are needed to close the round trip (see Fig. 3.12). To make the calculation easier, the reference plane is now located at the PCM rather than at the

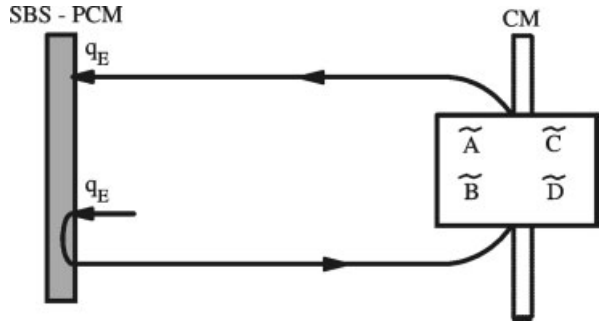

Figure 3.12. Round-trip model to calculate the eigensolutions of an SBS-PCR. The $\tilde{A}\tilde{B}\tilde{C}\tilde{D}$ matrix describes the entire resonator round trip including the SBS-PCM.

conventional mirror as before. The complete round-trip matrix reads

$$M_{\mathrm{rt}} \equiv \begin{pmatrix} A & B \\ C & D \end{pmatrix} = M_{\mathrm{back}} M_{\mathrm{CM}} \cdot M_{\mathrm{out}} \cdot M_{\mathrm{SBS-PCM}}$$

$$= \begin{pmatrix} \tilde{A} & \tilde{B} \\ \tilde{C} & \tilde{D} \end{pmatrix} \cdot \begin{pmatrix} 1 & 0 \\ -\dfrac{i\lambda}{\pi w_a^2} & -1 \end{pmatrix} \tag{11}$$

The radius of the Gaussian aperture a translates to a factor β ranging between 0 and 1. β indicates the ratio by which the incident beam radius w_i is reduced by the SBS-PCM:

$$w_r = \beta \cdot w_i, \qquad w_a^2 = \frac{\beta^2}{1-\beta^2} \cdot w_i^2 \tag{12}$$

w_r indicates the beam radius reflected off the PCM. The wavefront radius of the reflected beam is inverted $R_r = -R_i$. These equations for the beam radius and wavefront radius are derived from the general formulas in [52] for the special case of sharp focusing [52].

The round-trip self-consistency condition in the laser resonator has to be based on the *ABCD* law for optical systems containing phase conjugate optics, as described in Eq. (5). The eigensolution of this SBS-PCR consists of the following discrete eigenmode parameters in the plane of the SBS-PCM:

$$w_i = \sqrt{\frac{\lambda \tilde{B}}{\beta \pi}}, \qquad R_i = \frac{\tilde{B}}{\tilde{A}} \tag{13}$$

Let us consider this result for w_i for a β of 1 and compare it to the eigensolution for a conventional resonator where the PCM is exchanged with a flat conventional mirror

(CM). If we assume a typical stability parameter of $m = (A + D)/2 = 0.5$, a beam radius of $w_{\text{conventional}} = \sqrt{(\sqrt{4/3}\lambda B)/\pi}$ is yielded. It can be seen that this value is very similar to the beam radius at the PCM in the SBS-PCR. A closer look [53] confirms that the mode volume in a real PCR is comparable to that of corresponding stable resonators. Thus, different from common considerations (see, e.g., Ref. 30) a good extraction efficiency of the stored inversion by a transverse fundamental mode with a big cross section in the laser active material is not self-evident for PCRs. On the other hand, the wavefront curvature radius at one of the resonator mirrors resulting for the Gaussian beam with the lowest losses in a complex paraxial resonator is independent from the specific resonator design always provided by a PCM [53]. Thus, when large-diameter transverse fundamental mode eigensolutions are realized, they will suffer from lower losses in a PCR as compared to a conventional resonator. The experimental results of Skeldon and Boyd [22] and Giuliani [51] point out that this simple theory for the transverse mode works quite well at least when the injected start resonator mode is already close to the SBS-resonator theoretical eigensolution.

Figure 3.13 shows the eigensolution for an SBS laser with a variable lens (e.g., the laser rod in a solid-state laser) in two different configurations. It can be seen that for maintaining constant beam parameters the position of the PCM should be as close as possible to the variable lens. Perfect matching cannot be obtained, since the position of variable lens and PCM are not identical and the variable lens is a lens duct with a finite length itself. Both points lead to a change of the $\tilde{B}$ element in the round-trip matrix and therefore a change of w_r. Nevertheless, practically constant beam parameters are obtained for such an SBS-PCR—for example, for the full pump power range of solid-state lasers with a variable thermal lens.

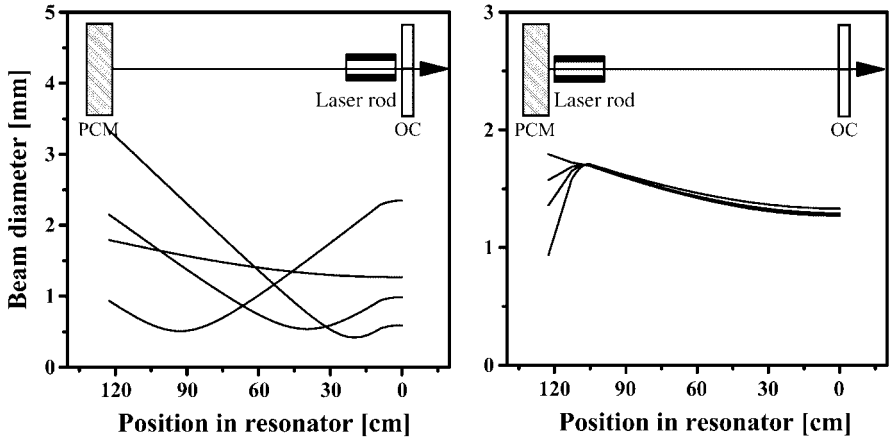

Figure 3.13. Eigensolution in an SBS-PCR with a $\beta = 1$ for four different dioptric powers of a pumped laser rod treated as a lens duct calculated with Eq. (13) for two extreme positions of the rod.

The perturbation stability of such an SBS-PCR can be characterized by using the results of Eq. (11) and Eq. (13) in Eq. (9). The growth rate results in

$$\left|\frac{\Delta q_E}{\Delta q^*_{\text{start}}}\right| = \beta^2 \tag{14}$$

Thus, perturbation stability is yielded for the SBS-PCM with a $\beta < 1$. The confined solution in the case of an infinitely wide aperture with $\beta = 1$ will be marginally perturbation stable only. From Eq. (14) one can deduce that a deviation Δw_1 from the beam radius w_i and ΔR_1 for the wave front radius R_i will yield $w_i + \Delta w_2$ and $R_i + \Delta R_2$, respectively, after one round trip.

$$\begin{aligned} \Delta w_2 &= -\Delta w_1 \\ \Delta R_2 &= -\Delta R_1 \beta^2 \end{aligned} \tag{15}$$

The wavefront radius will converge toward the eigenmode radius R_r, but the beam radius once perturbed will oscillate between the two solutions $w_i + \Delta w_2$ and $w_i - \Delta w_2$ around the eigensolution w_r. If this can be observed, it is dependent on the influence of a possibly existing superposed start resonator mode. Giuliani et al. [51] found at least some indication for this peculiar double round-trip mode. This should not be mixed up with the type of double round-trip eigenmodes which is obtainable in ideal PCRs.

Another special feature of SBS-PCRs is that the sensitivity of the mode radius against fluctuations is independent of its actual size. The eigenmode beam radius w_i at the PCM for a $\beta = 1$ is expressed as follows for a resonator of the length L; $w_i^2 = (2\lambda L g_2)/\pi$ using the equivalent g parameters of the resonator. The mode size sensitivity can then be expressed as

$$\frac{\partial w_2^2}{w_i^2} = \frac{\partial g_2}{g_2} \tag{16}$$

Stable conventional resonators where big mode sizes are typically achieved at the rim of stability regions suffer from strong fluctuations if geometrical resonator parameter changes occur. However, the mode size sensitivity of an SBS-PCR is directly proportional only to the mode size variation, and it does not depend on the geometrical resonator parameters.

There is not much literature on the experimental observation of higher order modes in PCRs (see, e.g., Refs. 48 and 54 for theoretical investigations). In Ref. 54 it is shown that PCRs with complex elements—for example, a Gaussian aperture in front of an PCM as the SBS-PCR—have real confined Gaussian–Hermite higher-order eigenmodes.

Of course most resonators will exhibit hard apertures as for limited mirror sizes or boundaries of the active material. In these cases only numerical investigations yield

satisfactory results for the eigenmodes. Numerical calculations were presented, for example, in Refs. 47 and 55. We will not discuss this issue here, but it should be mentioned that PCRs with hard apertures show lower round-trip losses and better beam quality compared to conventional resonators with hard apertures.

A PCR can compensate for intracavity phase distortions. Therefore it is a good concept especially for high-brightness solid-state lasers where the strong thermal load can be a big obstacle when realizing excellent beam qualities. The degeneracy of modes of an ideal PCR does not apply in real PCRs with apertures. An SBS-PCR exhibits a soft aperture in the SBS mirror generated by the transversely varying incident field. The beam radius of the discrete eigensolution of an SBS-PCR has a dimension similar to that of modes in stable resonators of the same interior.

A PCR always is the resonator with minimum loss as compared to conventional resonators with the same interior but arbitrary curvature of the replacing conventional mirror. With apertures the desired mode in the PCR can be determined. The sensitivity of the realized eigenmode then is independent from the actual size of the mode itself in contrast to the situation in stable resonators.

3.4 *Q*-SWITCH VIA STIMULATED BRILLOUIN SCATTERING

The following three sections concentrate on the principle of function of the sf-SBS laser introduced in Section 3.2 and give design rules for its setup. The performance data given in these sections were mostly measured with the laser setup depicted in Fig. 3.14. The laser heads were flash lamp pumped solid-state laser heads inhibiting either a Nd:YALO or a Nd:YAG rod.

The length of the SBS resonator is given by the distance of the focus between the two telescope lenses and the output coupler M1. The length $L_B = c/2\nu_B$ is called Brillouin length, where ν_B denotes the Brillouin frequency of the hypersound wave. This definition will become more evident in Section 3.5. Most of the discussed experiments were performed with SF_6 as SBS medium. It showed a Brillouin frequency of $\nu_B = 240\,\text{MHz}$ [56] and thus a corresponding Brillouin length of $L_B = 62.5\,\text{cm}$.

Solid-state lasers typically start to oscillate in the spiking regime, because solid-state active materials typically have considerably longer fluorescence lifetimes τ than the lifetime of the photons in the resonator τ_R. Therefore in solid-state SBS lasers a spike will grow up in the start resonator after pumping for time t_s. At this time the active material contains the threshold inversion density $\Delta n_{t,\text{start}}$ related to the start resonator:

$$\Delta n_{t,\text{start}} = \Delta n(t_s) = \frac{-\ln\left(\sqrt{R_{\text{start}}R_{\text{oc}}} \cdot V\right)}{\sigma l} \tag{17}$$

The spike power continues to grow in the start resonator until the SBS threshold is reached. Then the SBS reflectivity increases rapidly. This increase happens in a

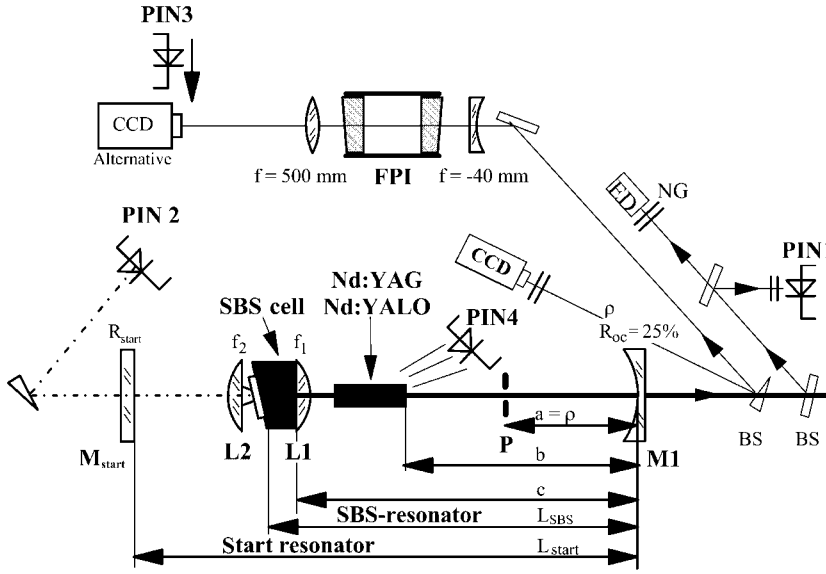

Figure 3.14. Scheme of the experimental setup. PIN denotes photodiodes, CCD a CCD camera, FPI a Fabry–Perot interferometer.

much shorter time than the *Q*-switch-pulse duration. Thus, a switch of the laser action occurs from the start resonator to the SBS resonator, and a *Q*-switch pulse is emitted out of the SBS resonator. If the SBS threshold is not reached by the spike power, the SBS mirror is not activated and thus the laser operates in the spiking regime only. Since the duration of the spike is short compared to the pump duration and assuming only negligible inversion depletion at the leading edge of the spike, the initial inversion for the *Q*-switch pulse is approximately $\Delta n_{t,\mathrm{start}}$. Thus the *Q*-switch pulse energy E can be derived as given in Ref. 57:

$$E(R_{\mathrm{start}}) = \frac{h\nu \cdot \pi w^2}{2\sigma} \cdot \ln\left(\frac{1}{\sqrt{R_{\mathrm{SBS}} R_{\mathrm{oc}}}}\right) \cdot \ln\left(\frac{-\ln\left(\sqrt{R_{\mathrm{start}} R_{\mathrm{oc}}} \cdot V\right)}{\Delta n_f \cdot \sigma \cdot l}\right) \tag{18}$$

$$\Delta n_i - \Delta n_f = \Delta n_{t,\mathrm{SBS}} \ln\left(\frac{\Delta n_i}{\Delta n_f}\right) \tag{19}$$

$$\Delta n_{t,\mathrm{SBS}} = \frac{-\ln\left(\sqrt{R_{\mathrm{SBS}} R_{\mathrm{oc}}} \cdot V\right)}{\sigma l}$$

σ denotes the emission cross section of the laser active material, ν the laser frequency, R_{SBS} the reflectivity of the SBS mirror, R_{oc} the reflectivity of the output coupler, V the single-pass loss of the start resonator, l the geometrical length of the

laser crystal, w the radius of the laser mode in the laser rod, and Δn_f the residual inversion density after the decay of the Q-switch pulse. Δn_f is connected with the initial inversion and the threshold inversion density by a transcendental equation where $\Delta n_{t,\mathrm{SBS}}$ denotes the threshold inversion density of the SBS resonator with a reflectivity R_{SBS} of the SBS mirror. Equation (18) shows the correlation of the Q-switch pulse energy with the reflectivity R_{start} of the mirror $\mathrm{M_{start}}$ and the spike onset time. Smaller reflectivities R_{start} lead to longer onset times of the first spike, because a higher inversion density is needed to come above threshold. Consequently, this bigger amount of stored inversion leads to higher pulse energies.

The Q-switch pulse energy can be calculated from Eq. (18) together with the solution of the transcendental Eq. (19) (calculation method I in Fig. 3.15). Another way to compute the pulse energies is the numerical solution of the rate equations for the inversion density in Nd:YAG together with the rate equation for the light intensity (calculation method II in Fig. 3.15) (see Ref. 58 for details). A constant reflectivity of the SBS mirror $R_{\mathrm{SBS}} = 80\%$ was assumed, following former measurements with beam splitters inside the resonator.

The deviation of the calculated pulse energy from the measured one for bigger values of R_{start} above 40% probably stems from the higher effective reflectivity of the combination of SBS mirror together with mirror $\mathrm{M_{start}}$.

A theoretical description of the Q switch in a slightly different SBS laser was given in Ref. 35, too.

The Q-switch process can be observed in detail by measuring the synchronized signals at PIN1 and PIN2 (see. Fig. 3.16). The time when the SBS mirror starts to

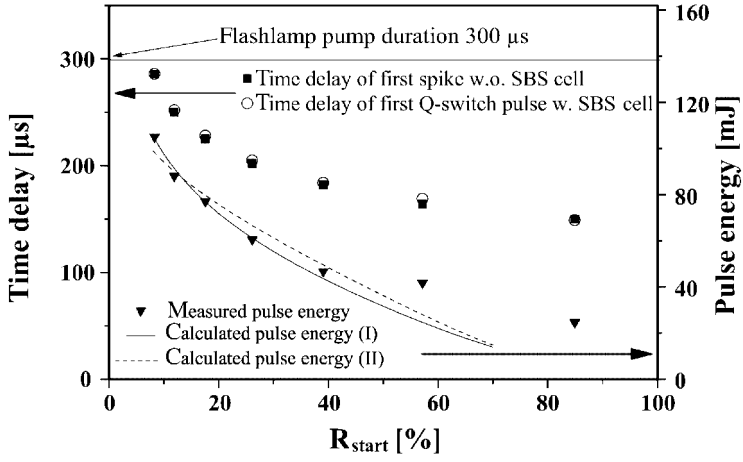

Figure 3.15. Measured onset times of the first spike of the start resonator without SBS cell and of the Q-switch pulse with SBS cell filled with SF_6 at 20 bar as a function of the reflectivity R_{start} of $\mathrm{M_{start}}$. Additionally, the measured and calculated pulse energies are shown. The position of the resonator elements were: $a = 200$ cm, $b = 451$ cm, $c = 477$ cm.

reflect remarkably can be determined from the periodicity of the modulation of the two signals of the start and SBS resonator. In the diagram at the bottom of Fig. 3.16, first one period can be addressed to four modulation peaks in the signal measured at PIN2. After the switch to the SBS resonator, the fourth intensity maximum appears together with the first in the signal at PIN2. The four-fold modulation within one period is changed to a three-fold modulation within one period because of the change in the effective resonator length from $4L_B$ to $3L_B$ and the corresponding round-trip times, respectively.

As can be seen from Fig. 3.17, the *Q*-switch-pulse energy seems to be independent of the threshold of the used SBS material. The SBS thresholds of xenon, CO_2, and SF_6 were measured with a single longitudinal *Q*-switched Nd:YAG laser

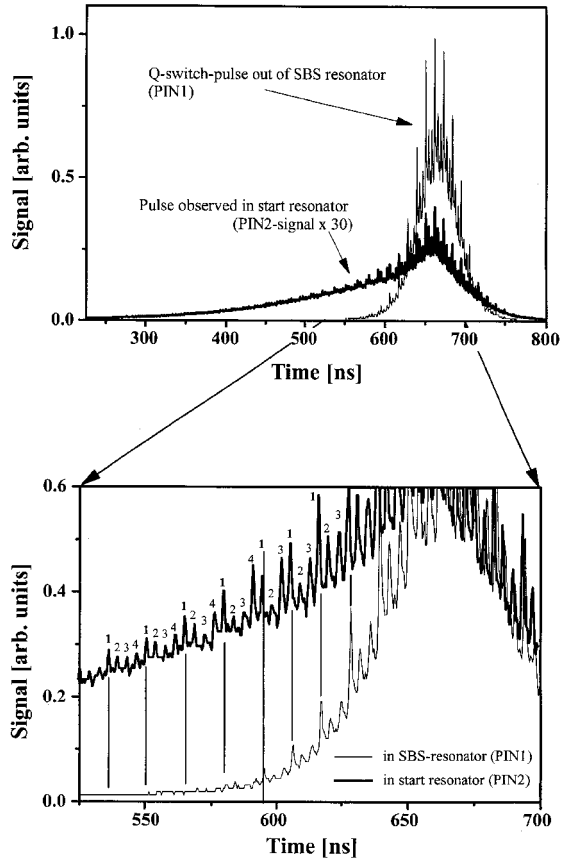

Figure 3.16. Signals detected at PIN1 and PIN2. The *Q*-switch is clarified by the periodicity in the round-trip times of the signals. This measurement was made with xenon as SBS material. The lengths of the start and SBS resonator were tuned to the Brillouin length of xenon, $L_B = 53.6$ cm: $L_{\text{start}} = 4L_B$ and $L_{\text{SBS}} = 3L_B$. The reflectivity of the start resonator mirror was 50%.

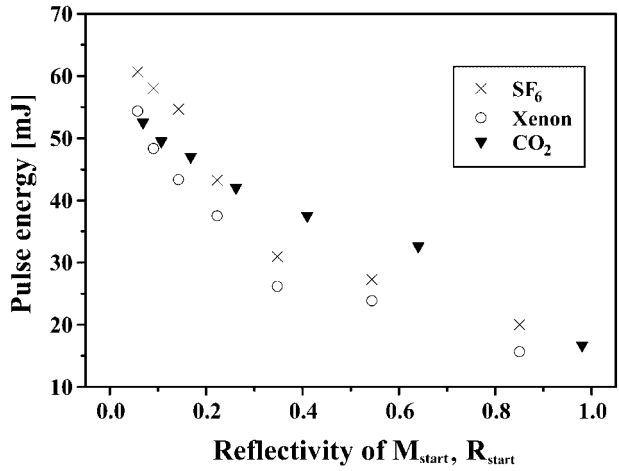

Figure 3.17. Measured pulse energies for three SBS materials as a function of the reflectivity R_{start} of M_{start}.

with a pulse duration of 30 ns and a bandwidth of 100 MHz to be 3.9 mJ, 6 mJ, and 10 mJ (Ref. 56 and previous chapter). On the other hand, from Eq. (18) we can see that the pulse energy is a function of R_{SBS}, which is a function of the threshold of the SBS mirror. But because the SBS threshold inside a resonator is reduced as explained in the next section by Brillouin enhanced four-wave mixing (BEFWM), these SBS mirrors are operated far above threshold. In this case, R_{SBS} becomes more or less the same for the three materials.

3.5 RESONANCE EFFECTS BY INTERACTION OF START RESONATOR MODES WITH THE SBS SOUND WAVE

The SBS threshold can be reduced by operating the SBS cell inside a resonator. This reduction is even necessary to operate most of the gaseous SBS materials in a laser oscillator since the SBS Q switch starts from spiking with low powers. The reduction of the threshold can be explained by a resonant generation of the sound wave via Brillouin enhanced four-wave mixing (BEFWM) of at least two longitudinal start resonator modes of the frequencies ν and $\nu + \Delta\nu$ with $\Delta\nu = \nu_B$. They act as two pump fields, one signal field, and the conjugate field (Fig. 3.18). This BEFWM takes place during the beginning of the spike oscillation in the start resonator.

The driving force of the sound wave is proportional to $\nabla^2(E^2)$, with E being the total electrical field in the SBS medium. For an effective energy transfer from the electrical field to the sound wave, a beat signal with a frequency within the bandwidth of the sound wave and with the velocity of the sound wave has to be generated. Thus, only $\mathcal{E}_2^* \cdot \mathcal{E}_3$ and $\mathcal{E}_1 \cdot \mathcal{E}_4^*$ out of the six beat terms of E^2 transfer energy to the sound wave (see Fig. 3.18, see Ref. 23 for details). The velocity of the

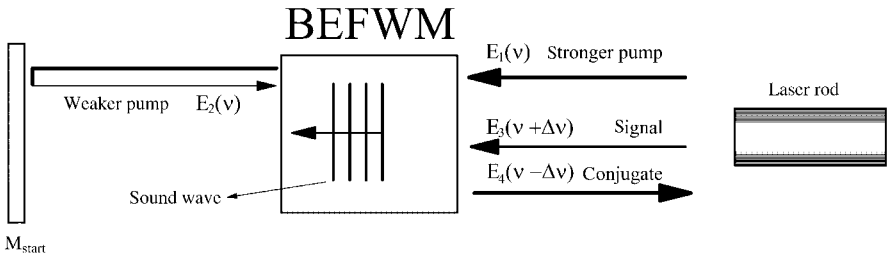

Figure 3.18. Scheme of the Brillouin enhanced four-wave mixing (BEFWM) in the start resonator.

beating ν_{beat} of E_2 and E_3 reads

$$\nu_{\text{beat}} = \frac{\Delta\nu_{\text{start}}}{2\nu_L}\frac{c}{n} = \frac{\lambda_{L,n}}{2}\Delta\nu_{\text{start}} \tag{20}$$

ν_L denotes the light frequency, $\lambda_{L,n}$ denotes the light wavelength in the SBS medium with the refractive index n, and $\Delta\nu_{\text{start}}$ denotes the spectral distance of the longitudinal modes in the start resonator. This leads to a wavelength of the beat signal λ_{beat}:

$$\lambda_{\text{beat}} = \frac{\nu_{\text{beat}}}{\Delta\nu_{\text{start}}} = \frac{\lambda_{L,n}}{2} \tag{21}$$

The corresponding quantities for the sound wave read [59]

$$\nu_{\text{sound}} = \frac{\nu_B}{2\nu_L}\frac{c}{n} \tag{22}$$

$$\lambda_{\text{sound}} = \frac{\nu_{\text{sound}}}{\nu_B} = \frac{\lambda_{L,n}}{2} \tag{23}$$

The beating of E_2 and E_3 and the back traveling sound wave have the same direction as well as the same velocity and wavelength if the spectral distance of the start resonator modes $\Delta\nu_{\text{start}}$ equals the Brillouin frequency $\Delta\nu_{\text{start}} = \nu_B$. In this case the beating of the longitudinal modes of the start resonator can couple to the sound wave most efficiently. Hence the resonant start resonator length should fulfill the condition

$$L_{\text{start}} = k\frac{c}{2\nu_B} \quad \Rightarrow \quad \Delta\nu_{\text{start}} = \frac{c}{2L_{\text{start}}} = \frac{\nu_B}{k} \tag{24}$$

Then the spectral distance $\Delta\nu$ given in Fig. 3.18 can become $\Delta\nu = k^*\Delta\nu_{\text{start}} = \nu_B$. The case of $k = 1$ represents the elementary Brillouin length $L_B = c/2\nu_B$. Higher numbers of k require beating between every kth longitudinal mode to drive the sound wave resonantly.

The sound wave generated by the fields E_2 and E_3 scatters the pump beam 1 into the conjugate beam 4. The beating of the fields 1 and 4 amplifies the sound wave and leads to an increasing intensity of the conjugate beam. This is equivalent to an increasing reflectivity of the SBS mirror. A distinct attenuation of E_2 takes place. This enables the switching from BEFWM to SBS in the description of the PCM. Then, only the fields E_1 and E_4 are of significant importance in the resonator. The scattering of the weaker pump E_2 into the signal beam E_3 is also possible, but this process has only a low efficiency as pointed out in Refs. 23 and 60.

Figure 3.19 shows how the ignition of the SBS mirror and consequently the Q-switch operation of the SBS-laser oscillator can be achieved best by choosing a resonant-start resonator length that is a multiple of the particular Brillouin length. If the start resonator length is too far from this resonant length, the laser operates in spiking only. In those cases the beat frequencies of the start resonator modes are spectrally too far away from ν_B to stimulate the sound wave in the SBS mirror. For the measurements of Fig. 3.19 the length of the start resonator in an Nd:YALO SBS-laser oscillator was varied. The pulse energy, its standard deviation, the longitudinal mode frequencies, and their beat frequencies were measured. While varying the start resonator length, it was assured that the start resonator remained stable. Also, an almost constant fundamental mode volume in the laser rod was used by setting the second telescope length appropriately (see Fig. 3.20). The suspension of the Q switch at the resonator lengths $L_{\text{start}} \approx 4L_B$ (SBS cell in the middle of the start resonator) can be explained by two counterpropagating sound waves in the SBS cell [8, 61] which are the result of a BEFWM without an effective reflectivity [62].

Working with liquid SBS materials, this resonance behavior of the start resonator length does not have to be that distinct and can even vanish. For the same start resonator length the ratio of the Brillouin line width and spectral width of the longitudinal modes in the start resonator will be bigger. An efficient generation of the sound wave becomes possibly independent of the start resonator length L_{start} if the Brillouin gain line overlaps with the beat frequency of the longitudinal modes which is closest to the Brillouin frequency: $k^* \Delta\nu_{\text{start}}(L_{\text{start}}) \approx \nu_B$.

3.6 LONGITUDINAL MODES OF THE LINEAR SBS LASER

The longitudinal mode spectrum of the sf-SBS laser is based on two major mechanisms. One is the Doppler shift at the moving sound wave grating in the SBS mirror, and the other is ordinary constructive interference of modes with frequencies $n*c/2L$. Section 3.6.1 concentrates on the first mechanism, whereas Sections 3.6.2 and 3.6.3 discuss interactions between the two mechanisms. Section 3.6.4 presents the influence of SBS materials with different acoustic decay times.

3.6.1 Transient longitudinal mode spectrum

The main structure of the longitudinal mode spectrum can be seen from Fig. 3.21 and Fig. 3.22. In Fig. 3.21, two typical longitudinal mode patterns detected with a

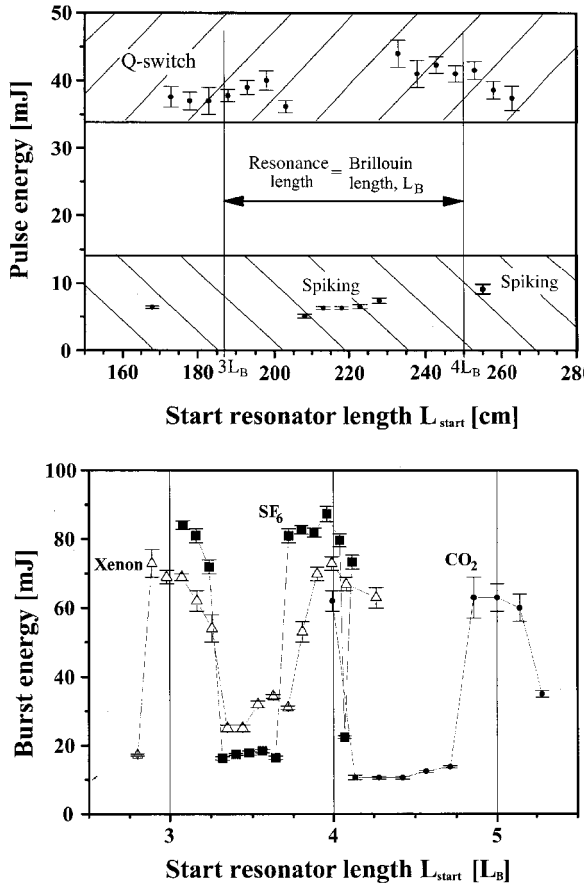

Figure 3.19. *Top:* Measured pulse energy of an sf-SBS laser as a function of the optical start resonator length for SF_6 as SBS material. Every data point is an averaged value over 500 measured single pulse energies. The error bars give the standard deviation. The length of the SBS resonator was $2L_B$. The two vertical lines indicate the third and fourth resonant start resonator length equal to $3L_B$ and $4L_B$. *Bottom:* Measured burst energy for the same laser as a function of the optical start resonator length normalized to the Brillouin length L_B of the used SBS materials xenon SF_6 and CO_2. Each data point is an averaged value over 500 measured burst energies. The error bars give the standard deviation. The lengths of the SBS resonator were $2L_B$ for SF_6 and xenon and $3L_B$ for CO_2.

Fabry–Perot interferometer (FPI) for SF_6 as SBS material is depicted. Figure 3.22 illustrates the results of such an FPI measurement for xenon ($L_{\text{start}} = 3L_B$, $L_{\text{SBS}} = 2L_B$) and CO_2 ($L_{\text{start}} = 4L_B$, $L_{\text{SBS}} = 3L_B$) as SBS materials. The FP interferograms show one free spectral range only. For all the three materials the dominant spectral distance between the longitudinal modes is the Brillouin frequency ν_B of the particular SBS material. In a few cases apart from the Brillouin frequency, other

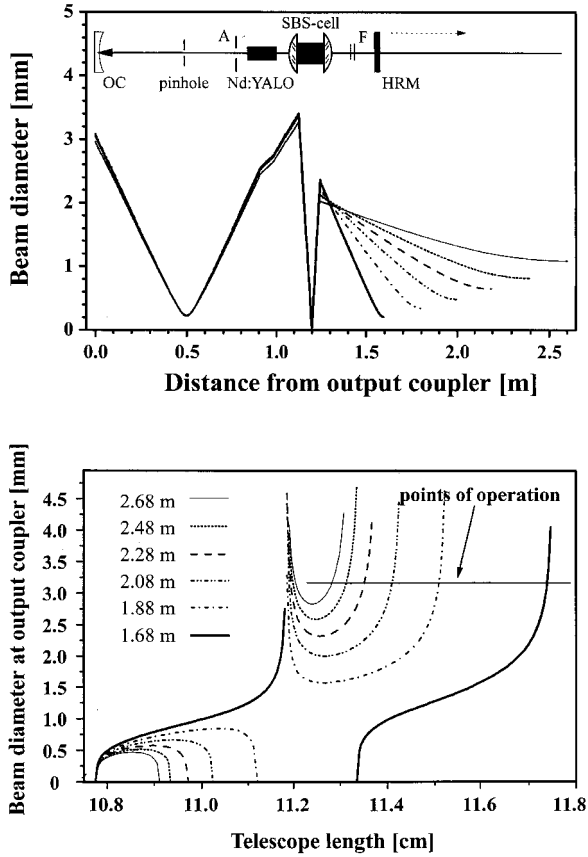

Figure 3.20. Calculated beam paths (*top*) and stability ranges (*bottom*) for different start resonator lengths of the SBS-laser oscillator using SF_6. The different realized points of operation for each resonator length are given by the horizontal line. The given resonator lengths are optical lengths. The beam path is calculated for the lowest-order eigensolution, a Gaussian beam, inside the stable start resonator. With the same formalism the beam diameter at the output coupler was calculated as a function of the telescope length. For details see Ref. 50.

frequency distances corresponding to the start resonator mode spacing $c/2L_{\text{start}}$ were determined. A measurement of such a case is shown in Fig. 3.21 on the right-hand side. The appearance of such pulses is statistical.

Figure 3.23 shows that the detected frequency distances in the interferograms are caused by the Brillouin shift only and are independent of the length of the SBS-resonator L_{SBS}. The also presented beat frequencies will be discussed in the next subsection. However, a more detailed observation reveals that the Brillouin shift of the SBS mirror is a function of the frequency of the driving force which is the beat signal of the longitudinal modes of the start resonator. If the start resonator is not

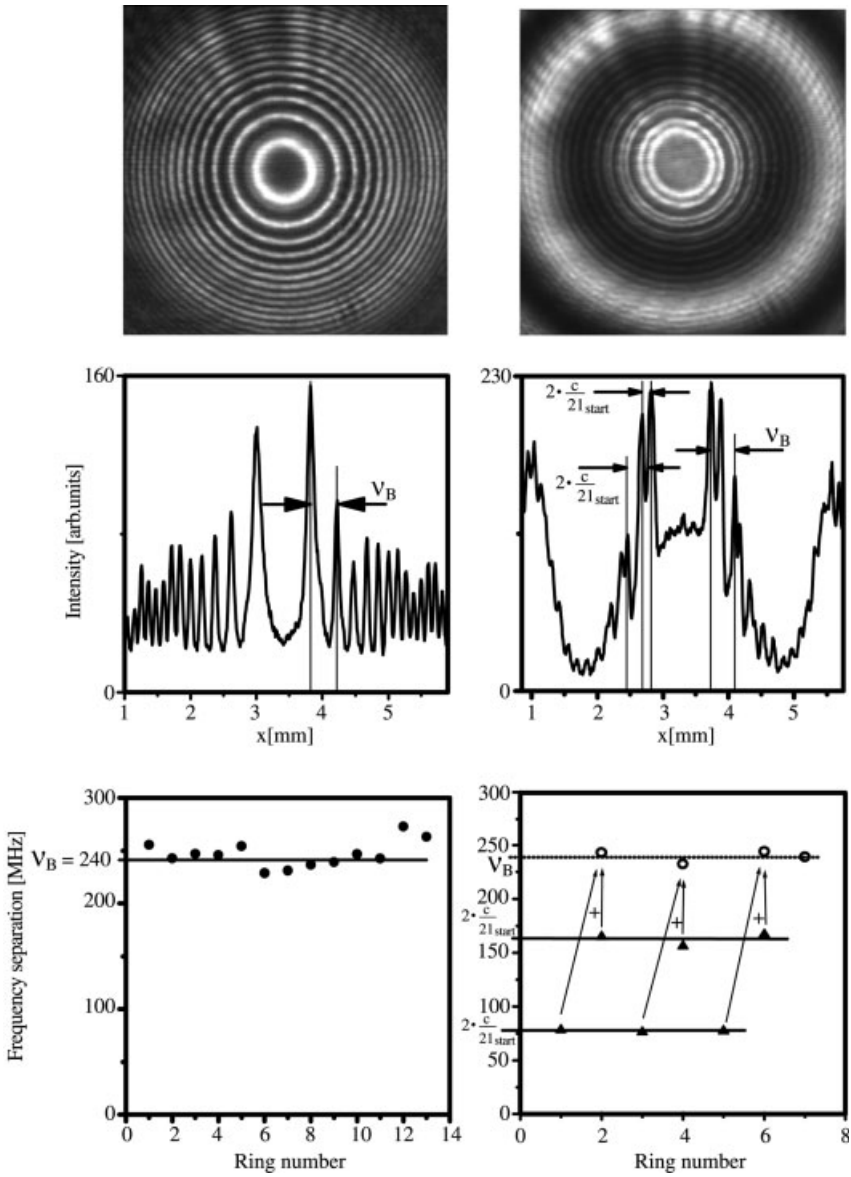

Figure 3.21. *Top* and *middle:* Typical Fabry–Perot interferograms (FPI) and their intensity cross sections taken for two different *Q*-switch pulses. The digrams at the bottom show the frequency distances of neighboring interference fringes (solid points). The SBS material was SF_6. Start and SBS resonator were tuned to the Brillouin frequency ($L_{start} = 3L_B$, $L_{SBS} = 2L_B$) *Left:* Only spectral distances equal to the Brillouin frequency ν_B can be detected. The shown range in the interferogram is totally within one free spectral range (3 GHz) of the FPI. *Right:* Additionally to the Brillouin frequency (every second ring), also frequency distances equal to the fundamental start resonator mode spacing $c/2L_{start}$ can be detected.

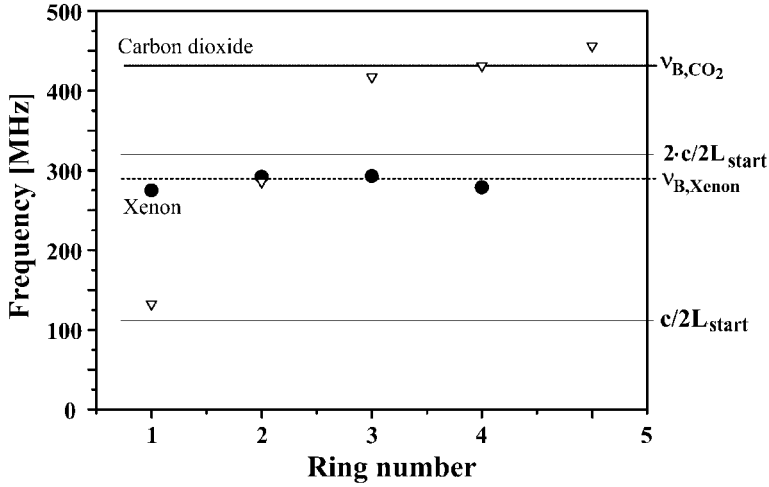

Figure 3.22. Frequency distances of neighboring interference fringes during one Q-switch pulse measured with the FPI similar to that in Fig. 3.21. The SBS materials were xenon and CO_2. Their Brillouin frequencies are marked as horizontal lines (CO_2 ——; xenon ----). For CO_2 also the spectral distance of the longitudinal modes of the start resonator are marked as thinner horizontal lines.

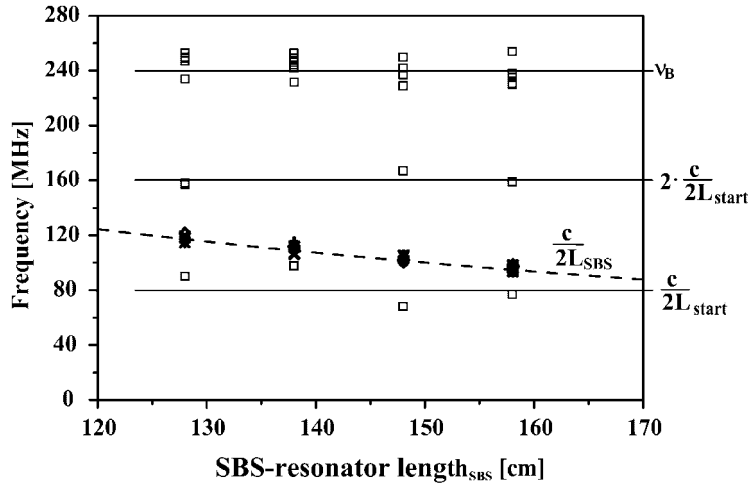

Figure 3.23. Frequency distances of neighboring interference fringes (□) during one Q-switch pulse as a function of different optical SBS-resonator lengths, measured with FPI. The horizontal lines denote the Brillouin frequency ν_B for the used SBS material SF_6 and the frequency distances of the start resonator modes $c/2L_{start}$ and $2 * c/2L_{start}$. The measured frequency distances ($*$, Δ, $\times$) of the beat frequencies from a Fourier transformation of the time distribution of the Q-switch pulses are also printed. The broken line corresponds to the calculated mode spacing of the SBS resonator $c/2L_{SBS}$.

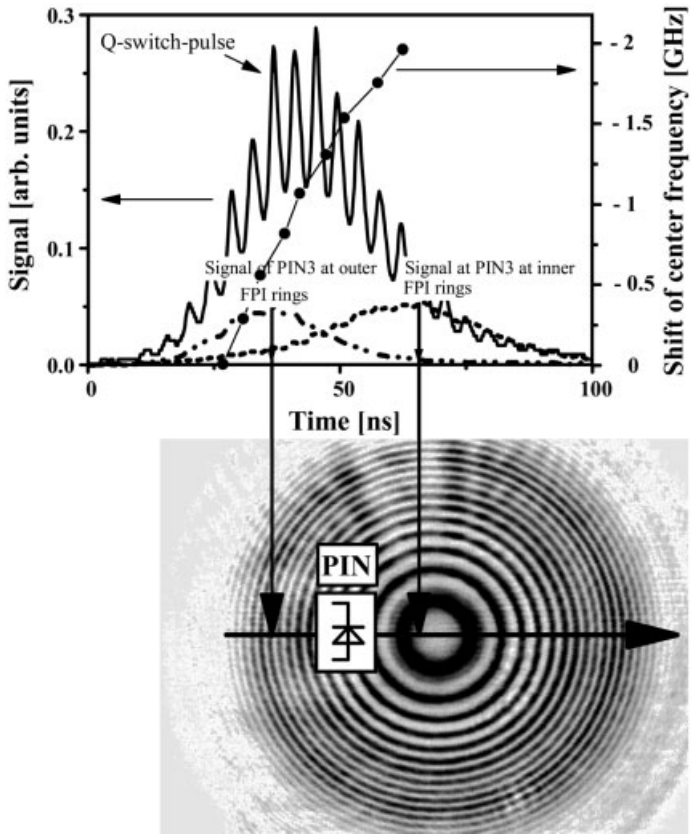

Figure 3.24. Measurement of the light frequency as a function of time during one *Q*-switch pulse. *Top:* The modulated time distribution belongs to the *Q*-switch pulse measured at the photodiode PIN1 (see Fig. 1). The curves in broken lines are the measured signals at the photodiode PIN3 at outer and inner FPI rings illustrated by the interferogram at the bottom. For nine positions of PIN3 the maximum of 100 averaged signals was determined and yielded a solid point in the diagram. The positions of PIN3 determined the frequency shift, which is depicted at the vertical axis.

exactly tuned to the Brillouin frequency, the spacing of the laser modes becomes a function of time. It is starting with the longitudinal mode beat frequency of the start resonator and is relaxing toward the Brillouin frequency of the used SBS material.

The longitudinal modes spaced by the Brillouin frequency are generated round trip by round trip due to the Doppler shift from the moving sound wave grating in the SBS mirror. One would expect that the spectrum becomes either wider and wider or just becomes shifted round trip by round trip. The latter description is in this case the appropriate one in contrast to the injected oscillators investigated by Damzen and co-workers [3, 4]. This will be clarified in the next subsection. Figure 3.24 shows the effect of the shifting mechanism. The mid-frequency of the longitudinal mode spectrum was measured during the *Q*-switch pulse (see Ref. 58 for details of the

measurement). In the top diagram of Fig. 3.24, each solid circle marks the temporal position of the maximum signal of a measurement with PIN3 of the setup of Fig. 3.14 at a certain position in the ring system corresponding to a certain frequency. It can be seen that the mid-frequency of the mode spectrum is shifted almost linearly during the Q-switch pulse.

The reasons for the temporal width of the signal detected with PIN3 are the averaging over 100 pulses and the size of the photodiode detector on one hand. But also several longitudinal modes exist simultaneously, leading to a "temporal overlap" of the modes, as will be shown in the next section.

3.6.2 Mode locking

Next to the effect of the SBS-threshold reduction by tuning the start resonator length, a resonant length $n \cdot L_B$ of the start resonator also leads to a common phase of the longitudinal modes. During the leading edge of the spike but before the SBS mirror is switched to high reflectivities, a generation of new longitudinal modes takes place. These new modes are generated via BEFWM with a spectral distance of ν_B. This mechanism can be observed in an interferogram taken with a highly reflecting ($R_{\text{start}} = 100\%$) start resonator mirror M_{start} as shown in Fig. 3.25. Although the laser was operated in the spiking regime without Q-switching, the influence of the

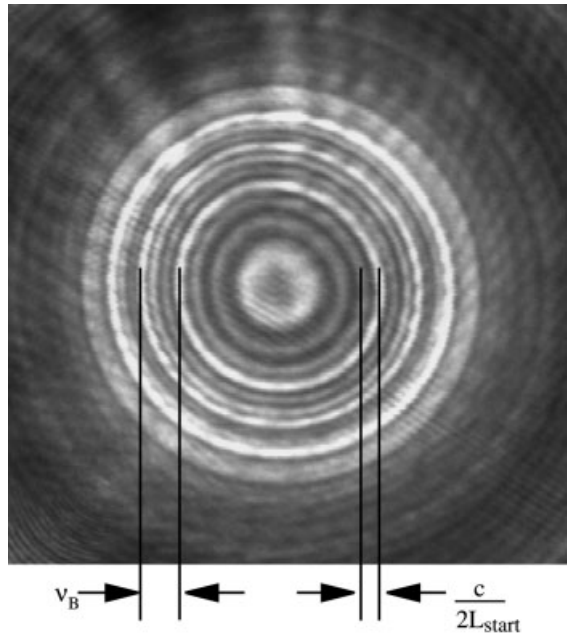

Figure 3.25. Interferogram of the longitudinal modes in the start resonator when using a highly reflecting start resonator mirror M_{start}. The lengths of the start and the SBS resonator were $L_{start} = 3L_B$, $L_{SBS} = 2L_B$. The measurement was performed with SF_6 as SBS material.

SBS cell can be clearly deduced from the higher intensities of those rings in Fig. 3.25 that have a spectral distance equal to the Brillouin frequency ν_B. Due to the chosen length of the start resonator $L_{\text{start}} = 3L_B$, ν_B equals the spectral distance of every third start resonator mode in this case.

As these strong modes with frequencies spaced by ν_B have arisen from each other, their phases are locked. After the Q switch, these locked phases can be preserved if the length of the SBS resonator is tuned to the Brillouin frequency, too. In this case the round-trip time in the SBS resonator is an integer multiple of the period of the sound wave. After one round trip of the light in the SBS resonator the maxima of the sound wave will be at the same position again as they have moved by the same multiple of the sound wave wavelengths. This phase locking leads to a regular modulation of the pulses in the tuned SBS resonators. The effect of seeding the SBS-resonator modes with a spectral spacing of the Brillouin frequency can also be seen from the dominant Brillouin beat frequency in the Fourier transform of the averaged pulses (see Fig. 3.26).

Due to an averaging over 50 pulses and a little jitter in the trigger time of the oscilloscope, the modulation is not as deep as for a single pulse. For a single pulse the modulation depth can be up to 90%. The longer the SBS resonator, the stronger the influence of the elementary round-trip time in the start resonator on the amplitudes of the beat frequencies in the pulse. In contrast to the pulses in the length-tuned SBS resonators of Fig. 3.26 in Fig. 3.27, the temporal profile of 50 averaged pulses of a nontuned SBS resonator is shown. The strongest beat frequency in this case is the inverse SBS resonator round-trip time of 92 MHz $= 1/11$ ns.

The interferograms showed that the Brillouin frequency ν_B is the dominant frequency spacing in the mode ensemble during one Q-switch pulse independent of the length of the SBS resonator (see Fig. 3.23). In some cases even the elementary mode spacing of the start resonator was obtained. The mode spacing of the SBS resonator, $c/2L_{\text{SBS}}$, is never been observed in the interferograms of any Q-switch pulse. The reason for this will be explained in the following section. However, the modulation periods in the pulses correspond well to the chosen SBS-resonator length as can be seen from the Fourier transform of the pulses in Fig. 3.23 (measured points along the broken theoretical curve).

The Brillouin frequency was not observed in the Fourier transform of the pulse intensities in Fig. 3.23. The Fourier transform contains the frequency distances of the absolute frequencies, and these beat frequencies can only be generated from simultaneously existing absolute frequencies. But outside the resonator the Brillouin shifted signals do not exist simultaneously in time and space. They are separated by the SBS-resonator round-trip time and the double SBS-resonator length, respectively. This is distinctively different from the injected oscillators realized by Damzen and co-workers [3, 4]. They injected the original frequency over the entire pulse duration into the oscillator so that a real increase in bandwidth is yielded. Due to the mode locking mechanism they observed short ps-pulses. But in the self-starting SBS laser case the start frequency is not continuously supplied so that the whole spectrum is shifted during the pulse duration but not broadened.

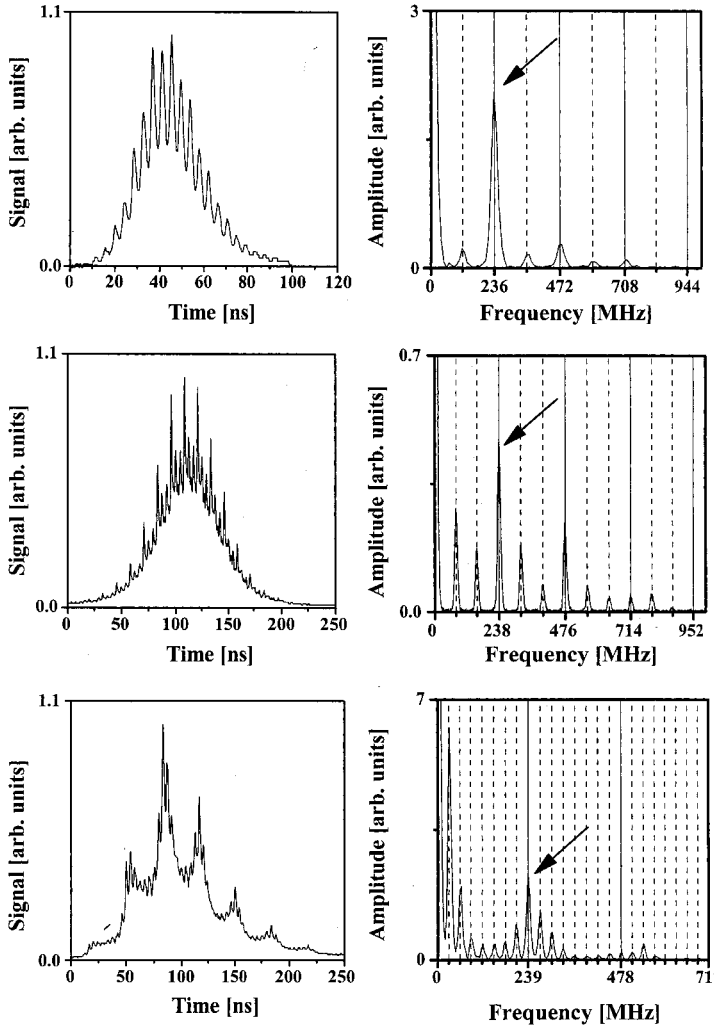

Figure 3.26. Measurement of averaged Q-switch pulses of SBS-laser oscillators with SF_6 as SBS material but different resonant resonator lengths. The ratios of the lengths of start and SBS resonator in units of $L_B = 62.5$ cm were: *Top:* 3:2 (Nd:YAG), *Middle:* 4:3 ($a = 50$ cm, $b = 132$ cm, $c = 162$ cm $= d$). *Bottom:* 9:8 ($a = 200$ cm, $b = 451$ cm, $c = d = 477$ cm). On the right-hand side the Fourier transform of the time distributions are shown. The broken lines denote multiples of the frequency spacing of the SBS resonator $\Delta\nu_{SBS} = c/2L_{SBS}$.

Besides the impact of the SBS-resonator length on the longitudinal mode structure, the longitudinal mode structure itself has an impact on the efficiency of the SBS reflectivity [61, 63]. We will not discuss this issue here in detail. But Fig. 3.28

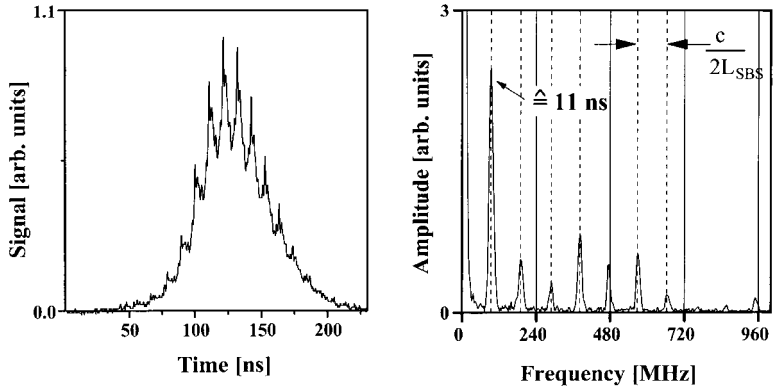

Figure 3.27. Time distribution and its Fourier transform of 50 averaged Q-switch pulses measured with an SBS resonator length $L_{\mathrm{SBS}} = 2.5L_B$. The SBS material was SF_6.

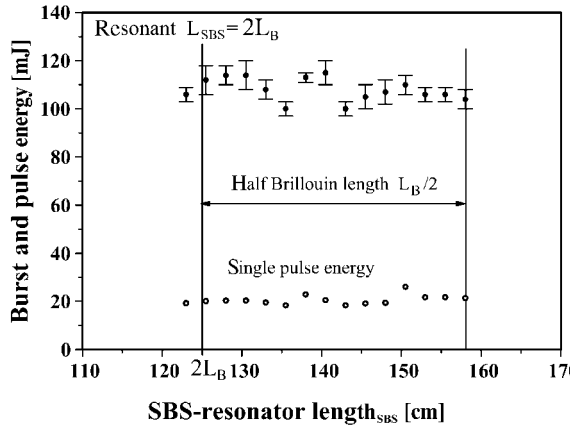

Figure 3.28. Measured pulse energies for different optical SBS-resonator lengths. Each point is an energy average over 100 pulses. The error bar denotes the measured standard deviation.

shows some experimental evidence that there is no significant impact on the laser efficiency found while tuning the start resonator length (see Fig. 3.28).

3.6.3 Analytical pulse shape description

The complex electrical field $\mathcal{E}(t)$ of the Q-switch pulse can be described by the sum of plane wave fields with equidistant frequencies $\omega_m = \omega_0 + m \cdot \Delta\omega$:

$$\mathcal{E}(t) = \sum_{m=1}^{n} a_m \exp\left(i(\omega_m t + \theta_m)\right), \qquad E := \frac{1}{2}(\mathcal{E} + \mathcal{E}^*) \tag{25}$$

θ_k denotes the phase of the field component with the frequency ω_k and the real amplitude a_k. Time averaging of the electric field amplitude over the period $T_0 = 1/\omega_0$ leads to the following intensity of the Q-switch pulse with a Gaussian pulse shape of the duration t_w (FWHM):

$$I(t) = \epsilon_0 c_0 \overline{E^2} = \epsilon_0 c_0 \mathcal{E}(t) \cdot \mathcal{E}^*(t) \cdot \exp\left(-\frac{t^2}{t_w^2}\ln(2)\right) \tag{26}$$

where c_0 denotes the vacuum light velocity whereas ϵ_0 is the vacuum permittivity. For a spectrum of n frequencies the intensity is given as

$$I(t) = \epsilon_0 c_0 \left\{\sum_{m=1}^{n} a_m^2 + 2\sum_{m=1}^{n-1}\left[\left(\sum_{j=1}^{n-m} a_j a_{j+m}\cos(\theta_j - \theta_{j+m})\right)\cos(m\cdot\Delta\omega t)\right]\right\} \times \exp\left(-\frac{t^2}{t_w^2}\ln(2)\right) \tag{27}$$

It can be seen that only the difference frequencies (beat frequencies) and no absolute frequencies ω_k are contained in this intensity anymore. Consider a mode series consisting of every kth mode of the longitudinal modes of a resonator. The frequencies of this mode series $\omega_{k\times p}$ have a spectral distance of $\omega_{k\times p} - \omega_{k\times(p+1)} = k\cdot\Delta\omega$ (k and p being integers). If there exists a locking mechanism for their phases, it will apply $\theta_{k\times p} - \theta_{k\times(p+1)} = \text{const.}$ for every integer p and every pulse. In this case in Eq. (27), $\cos(\theta_{k\times p} - \theta_{k\times(p+1)})$ has the same value for every Q-switch pulse (e.g., 1). Other terms like $\cos(\theta_{k\times p+1} - \theta_{k\times(p+1)+1})$ in front of $\cos(k\Delta\omega)$ have different values since they are not supported by the locking mechanism.

If there is no locking mechanism for a mode series containing every kth mode, the phase angles are determined by the spontaneous laser emission. Then, for every mode pair and each pulse the difference $\theta_{k\times p} - \theta_{k\times(p+1)}$ has different values. The sum in front of $\cos(k\cdot\Delta\omega t)$ in Eq. (27) has different values for every pulse, too. Therefore the average for many pulse intensities of all the sums in front of $\cos(k\Delta\omega)$ approaches zero as a result. Consequently, in the Fourier transform the amplitude for $k\cdot\Delta\omega$ is approaching zero, too. On the other hand, in the case of locked modes the amplitude for $k\cdot\Delta\omega$ is strong since there is no cancellation. This is the explanation for the dominant beat frequency equal to the Brillouin frequency $k\cdot\Delta\omega = \nu_B$ and corroborates the explanation of the mode locking of the modes spaced by ν_B given in the last section.

Assuming that after every round trip with the duration t_{rt} a constant frequency shift ω_B is applied for all components of the field $\mathcal{E}(t)$, a time-dependent frequency $\omega_m(t)$ for the mth mode can be introduced. This frequency alters its value after each round trip in the resonator with the time duration t_{rt}.

$$\omega_m(t) = [\omega_0 + m\cdot\Delta\omega] - [\omega_B\cdot(N(t))] \tag{28}$$

where $N(t)$ is the number of the round trip at the time t counted from the beginning of the Q-switch pulse. But since the whole spectrum is shifted by the same amount ω_B, the frequency differences of the longitudinal modes remain the same. Therefore it can be shown by a straightforward calculation that under the assumption of such a shifting mechanism the intensity still has the form of Eq. (27). Consequently, the calculated pulse shapes of Eq. (26) are very similar to the measured pulse shapes if the correct amplitudes and phases are applied (see Figs. 3.29 and 3.30).

As has been explained, there is an identical phase angle for the longitudinal modes spaced by the Brillouin frequency if start and SBS resonator are tuned to the Brillouin frequency. If there are beat frequencies with a different spectral distance, their corresponding fields should have any arbitrary phase angle since there is no locking mechanism for them. Therefore, in the calculation the phases of the fields with an even index (it is even because $L_{\mathrm{SBS}} = 2L_B$) and a spectral distance of ν_B were chosen identical and the phase angles of the remaining fields with uneven index were chosen randomly.

It turns out that every observed pulse shape can be calculated in an optimal way following one of the two assumptions for two different cases. Either there exists only one strong amplitude at one frequency ω_k in a non-length-tuned SBS resonator or in

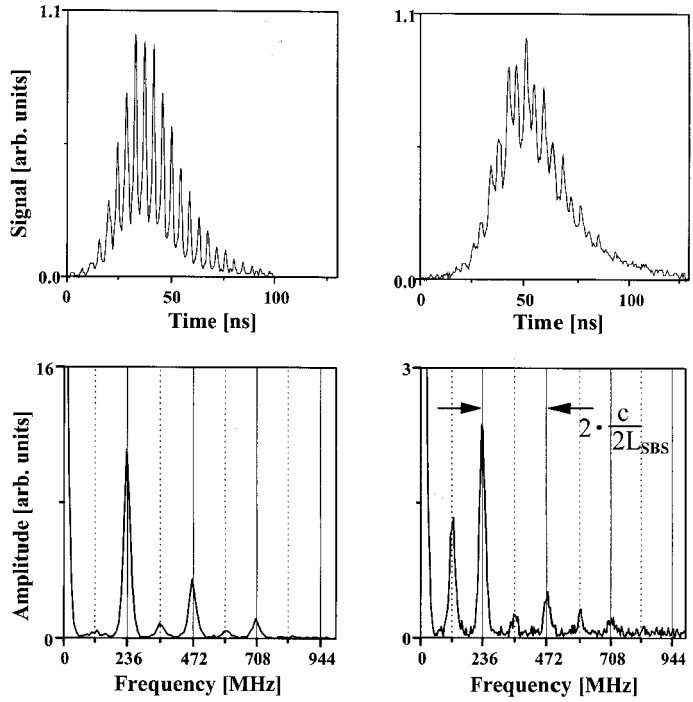

Figure 3.29. Two measured time distributions of Q-switch pulses from Fig. 3.21 and its Fourier transforms.

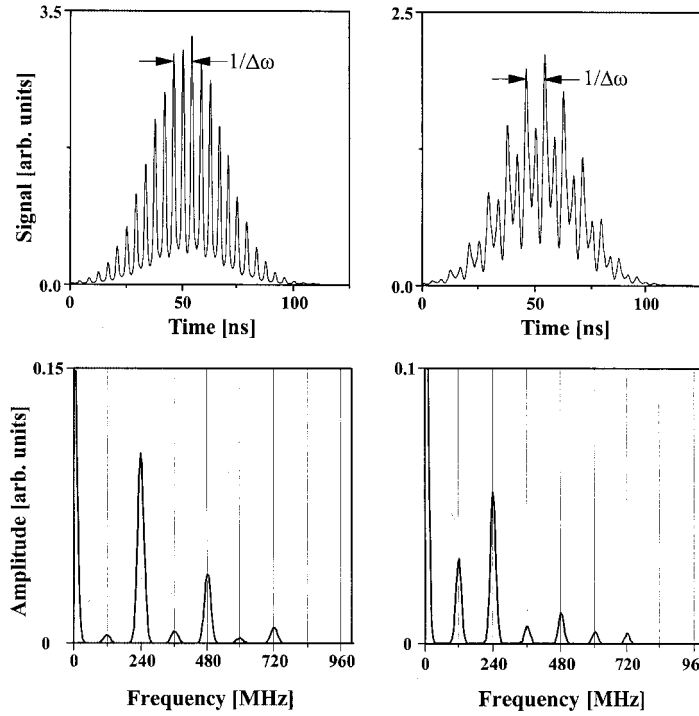

Figure 3.30. Two calculated time distributions of pulses and their Fourier transforms. To adapt the shapes of the pulses in Fig. 3.29, the amplitudes of the electrical fields are as follows: *Left:* $a_1 = 1, a_2 = 0.011, a_3 = 0.5, a_4 = 0.03, a_5 = 0.2, a_6 = 0.015, a_7 = 0.05$. *Right:* $a_1 = 1$, $a_2 = 0.15, a_3 = 0.27, a_4 = 0.03, a_5 = 0.03, a_6 = 0.015, a_7 = 0.02$. The phases of fields with an even number k are chosen randomly. For the uneven fields, $\Theta_k = 0$ applies.

a length-tuned SBS resonator there are one or two additional strong amplitudes with a spectral distance of the Brillouin frequency ν_B.

If there are longitudinal modes with frequency distances other than ν_B, they show such small amplitudes that they cannot be measured with the FPI. Because of the spectral resolution of 59 MHz of the FPI and the squaring of the fields in the measured intensity, these small amplitudes are part of the background of the measured signal (notice that the modulation of the FPI signals does not reach the 0 level).

3.6.4 Impact of acoustic decay time on longitudinal modes

So far we have not taken into account the specific threshold of the SBS material and the acoustic decay time of the sound wave grating. Low thresholds are especially interesting for CW applications. To the best of our knowledge, there has not been

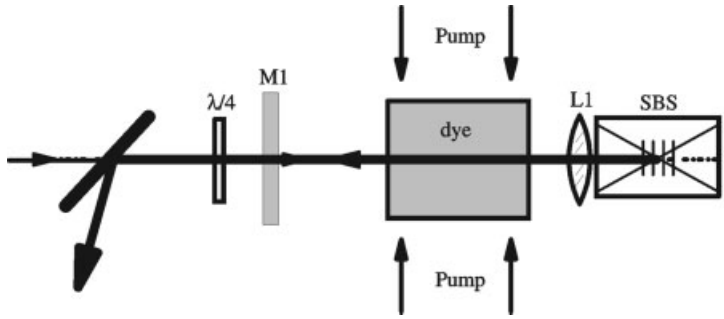

Figure 3.31. Layout of injected SBS-dye laser for investigations of impact of acoustic decay time on lasing process.

any CW-SBS-laser oscillator realized yet, and we are not going to discuss concepts for CW SBS lasers here. Up to now, typical materials for cw operation are photorefractive crystals (see Chapter 8). Low-threshold SBS mirrors are discussed in the previous chapter.

However, the acoustic decay time of the SBS material is also an issue for *Q*-switched SBS laser. Especially the impact of this decay time on the lasing process was investigated theoretically by Barrientos et al. [44] for an injected dye laser (see Fig. 3.31). They used a set of SBS equations assuming plane waves, narrow bandwidth for the SBS, and an SVE approximation for the electrical fields (see Section 2.2.1 in Chapter 2). The laser process is described by rate equations assuming absence of excited-state absorption, triplet-state formation, and amplified spontaneous emission as well as no scatter or diffraction losses.

The main characteristics of this injected oscillator in terms of impact of the decay time are also valid for the self-starting SBS laser. Four different decay times τ_B corresponding to four different SBS materials were investigated: 0.5 ns (*n*-hexane), 1.5 ns ($TiCl_4$), 3.5 ns (C_2F_6), and 8.5 ns ($CClF_3$). The round-trip time of the cavity was 7.3 ns. The duration of the injected pulses was 12 ns and the pulse energy was 300 mJ for the first three materials. For $CClF_3$ with the longest acoustic decay time the pulse energy was risen to 500 μJ.

The modulation period of the out-coupled intensity corresponds to the round-trip time t_{rt} of the SBS resonator. The shorter the decay time τ_B, the more distinct became the modulation (see Fig. 3.32). For decay times shorter than about one-fourth of the round trip, time termination of SBS and hence no laser output was found. For long decay times comparable to the round-trip period, steady-state oscillation was approached. Also, the shorter the decay time, the faster the reflectivity of the SBS mirror reacts. When the decay time becomes too long (in this investigation 4.4 ns), SBS becomes too transient. The SBS-threshold intensity is not reached, and no lasting laser oscillation takes place. If the injected pulse energy was elevated, the threshold would have been reached again.

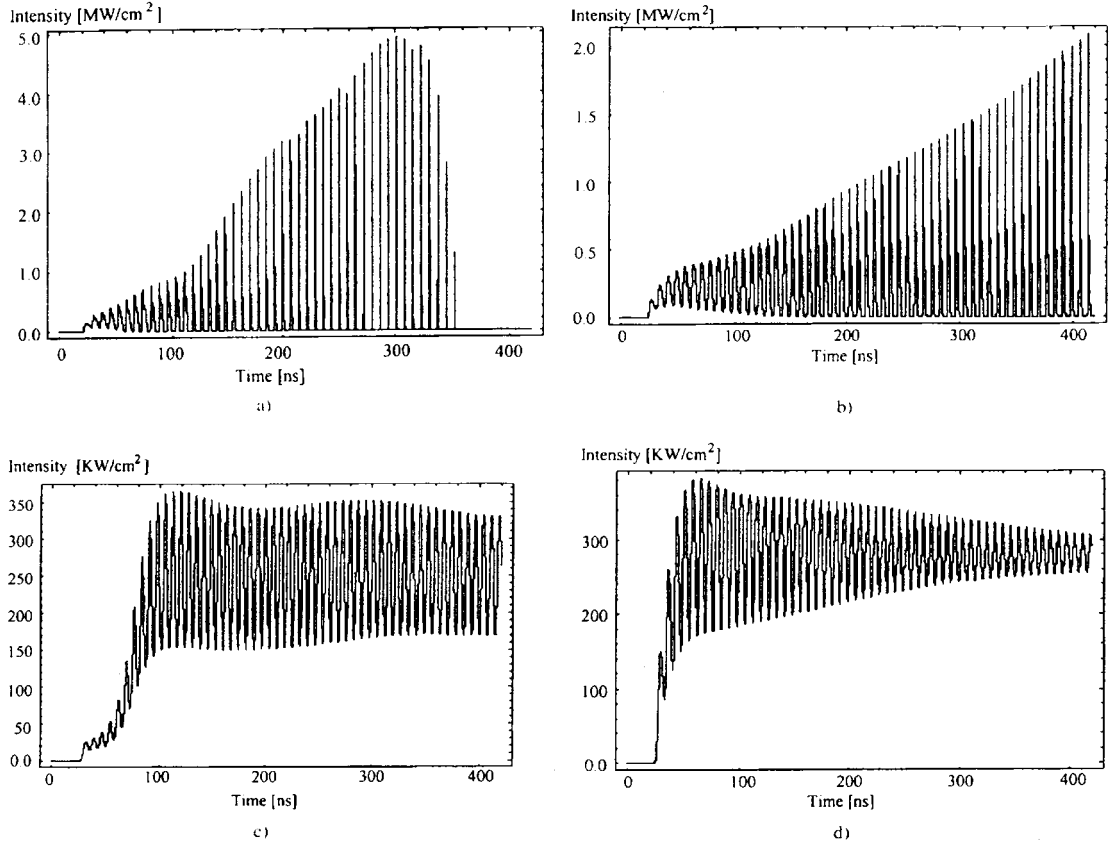

Figure 3.32. Calculated out coupled intensity as a result of a numerical simulation according to Ref. 44 for four different decay times: 0.5 ns (*n*-hexane), 1.5 ns ($TiCl_4$), 3.5 ns (C_2F_6), and 8.5 ns ($CClF_3$).

3.6.5 Summary

In Sections 3.4–3.6 the SBS mirror as part of the laser resonator has been explained with regard to its function as a simple device for *Q*-switching of laser oscillators. The *Q*-switch pulse parameters can be easily varied by a loss variation in the start resonator since the laser oscillation starts with the leading edge of a spike out of the start resonator. A length tuning of the start resonator is necessary to achieve a resonant generation of the sound wave grating in the SBS mirror. This way a threshold reduction for the SBS mirror via Brillouin enhanced for wave mixing (BEFWM) of the start resonator modes takes place. Without this length tuning, an SBS-laser oscillator with a gaseous SBS material will not operate in *Q*-switch regime but in spiking. The length of the SBS resonator does not seem to be important for the efficiency and stability of the *Q* switch, but has influence on the phases of the longitudinal modes. Due to the seeding process in the start resonator via BEFWM, phase locking can be achieved during the *Q*-switch pulse if a length tuning of start and SBS resonator has been performed. Due to the moving sound wave grating in the SBS mirror, the SBS-laser oscillator embodies a time-dependent mode spectrum with a decreasing center frequency of the longitudinal mode spectrum during the *Q*-switch pulse. Within a simple model the shape of the *Q*-switch pulses can be calculated using a few longitudinal modes only. Their frequencies are related to the length of the SBS resonator, the correct phase angles must be considered, but the Doppler shift of the SBS mirror has no influence on the pulse shape. Shorter acoustic decay times lead to stronger modulations in the out coupled intensity. Laser oscillation may break down if the acoustic decay time is shorter than one-fourth of the round-trip time of the SBS resonator.

3.7 HIGH BRIGHTNESS OPERATION OF THE LINEAR-SBS LASER

The two major reasons to use SBS mirrors in high-power laser oscillators are their phase conjugating properties on one hand and their nonlinear reflectivity to realize a very efficient *Q* switch for higher pulse energies on the other hand.

The thermal load in solid-state lasers limits their brightness. Due to the temperature dependence of the heat conductivity and the specific distribution of the heat generation inside the laser crystal, the deviation from the ideal parabolic refraction index profile will increase with increasing pump powers [64]. This leads to an increasing deterioration of the beam quality. Furthermore, in stable solid-state laser resonators with varying thermal lenses, the highest output power realizable at a given beam quality is limited by the strength of the thermal lensing [65]. The stability of the resonator becomes more and more problematic for higher pump powers. Phase conjugating resonators (PCRs) can compensate for these problems [49]. In this section we discuss the ability of the sf-SBS laser to realize high average output powers with a near diffraction-limited beam quality at a specific example.

This specific PCR with SBS mirror for high brightness output is a flashlamp-pumped Nd:YALO laser oscillator [27]. The schematic of the laser resonator and the

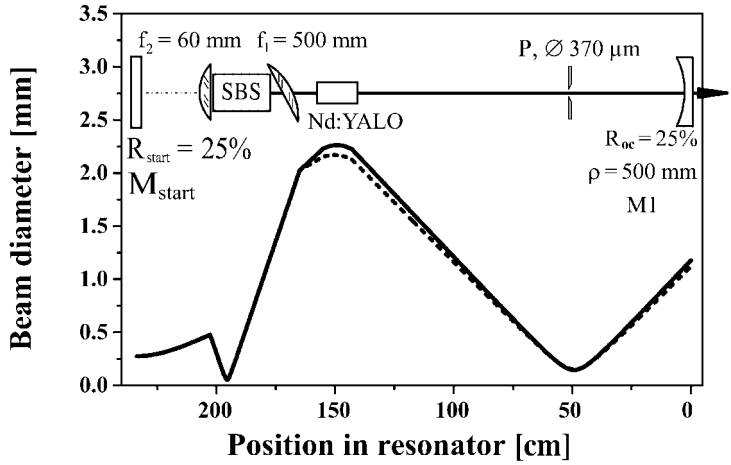

Figure 3.33. Scheme of the laser resonator. The distances of the resonator elements from the output coupler are as follows: pinhole P, 50 cm; laser rod's endface, 143 cm; lens L1, 165 cm; lens L2 depending on pump power; mirror M_{start}; 234 cm. The SBS cell is 30 cm long and 1 cm in diameter and is positioned directly in front of lens L2. The laser rod dimension is 7 mm × 120 mm with a doping level of 0.8 at%. The overall pump energy of the two flashlamps was 100 J at a pump pulse duration of 1 ms. The solid and broken curves, respectively, show the eigensolution for the stronger and weaker dioptric power of the laser rod thermal lens.

calculated eigenmodes regarding to the two dioptric powers of the thermal lens of Nd:YALO are shown in Fig. 3.33.

The design of this resonator is to be found in the peculiarities of PCRs: The degeneracy of modes in PCRs can lead to eigensolutions that build focuses on surfaces of the optical elements in the resonator which would lead to damage of these elements. This resonator design with a pinhole at the position of the beam waist and the rods aperture as second mode-selecting aperture does not allow for other than the transverse fundamental mode to come above threshold [66]. It particularly does not allow for any mode with a focus on one of the SBS-resonator elements. The mode diameter on the start resonator mirror is less crucial since the intensity in this resonator part is low. Furthermore, this set of apertures lifts the mode degeneracy in a way that a large transverse fundamental mode volume is realized, since this is the eigensolution with the lowest round-trip loss.

The SBS resonator is not an ideal PCR. To some extent, it is an SBS-PCR as discussed in Section 6.3 with a mode injected from the start resonator. This mode is more or less perturbed compared to the eigenmode of the SBS resonator. But guaranteed by apertures the eigenmode of the SBS resonator is close to the one of the start resonator. The pinhole in the resonator acts at least partially as a spatial filter. A fraction of the lens duct will have a focal length equal to the distance between laser rod and pinhole. Therefore, in addition to the condition of matching the curvatures at

the output coupler, it realizes a second loss mechanism for nonparabolic wavefront distortions of the transverse fundamental mode and supports the convergence of the eigensolution in the SBS resonator toward the high beam quality transverse fundamental mode.

3.7.1 Crucial components of the SBS laser Anisotropic materials allow for operation with linear polarized laser light without any additional polarizers, since the thermally induced birefringence becomes negligible compared to their naturally birefringence. Therefore in this example Nd:YALO was chosen as laser-active material.

The telescope enclosing the SBS cell benefits in four different ways. First, it reduces the coherence demands on the laser light for the SBS. The sharper the beam is focused, the stronger the reflectivity at each plane of the sound wave grating. Thus, less grating planes are necessary to reach a certain reflectivity, and hence a shorter interaction length results when using a sharper focusing [67]. Second, the telescope makes it possible to set up the start resonator with a large transverse fundamental mode beam diameter in the laser rod. For reaching a high efficiency and achieving a good discrimination of higher-order modes, a beam diameter of 4.4 mm in the laser rod was calculated and realized in this laser. The mode selection is achieved by the rod aperture of 7-mm diameter in combination with the pinhole P. The start resonator was set up for dynamically stable operation (see Fig. 3.34). Third, despite the large beam diameter inside the laser rod, a wide pump power range can be used by varying the distance of the two telescope lenses [28]. Fourth, using an anisotropic material such as Nd:YALO, the astigmatism of the thermally induced dioptric power of the laser rod (0.70 dpt/kW and 0.83 dpt/kW in this case) can be compensated by tilting the first telescope lens as a function of the pump power.

Although we have a phase conjugating resonator, the compensation of the astigmatism is necessary because the astigmatic thermal lens leads to a separation of the stability range of the start resonator in two ranges, one for each dioptric power. If these two stability ranges have no overlap, the start resonator becomes unstable. As a consequence, if the diffraction losses become too big, the start resonator will not reach threshold at all. This is avoided by the astigmatism compensation.

The focal lengths of the telescope lenses should be chosen for spot sizes not too small to avoid optical breakdown in the SBS material. Optical breakdown for gases is known to occur at intensities of $10^{11}-10^{12}$ W/cm^2 [68] for nanosecond pulses.

To avoid an optical breakdown at the pinhole plane, this resonator type can be evacuated around the pinhole. The pinhole was made of quartz glass. To obtain the maximum intracavity SBS-threshold reduction as pointed out in Section 3.5, the start resonator length should be chosen regarding to the Brillouin frequency. Here we have chosen the optical length of the start resonator to be $L_{\text{start}} = 4 * c/2\nu_B = 250$ cm ($\nu_B = 240$ MHz for the SBS material used, SF_6). The reason for choosing four times the mode distance is related to the design of the start resonator and the transverse mode size: The beam diameter at the pinhole should not be too small to accommodate high intensities. Consequentially, for this kind of a start resonator design, the large

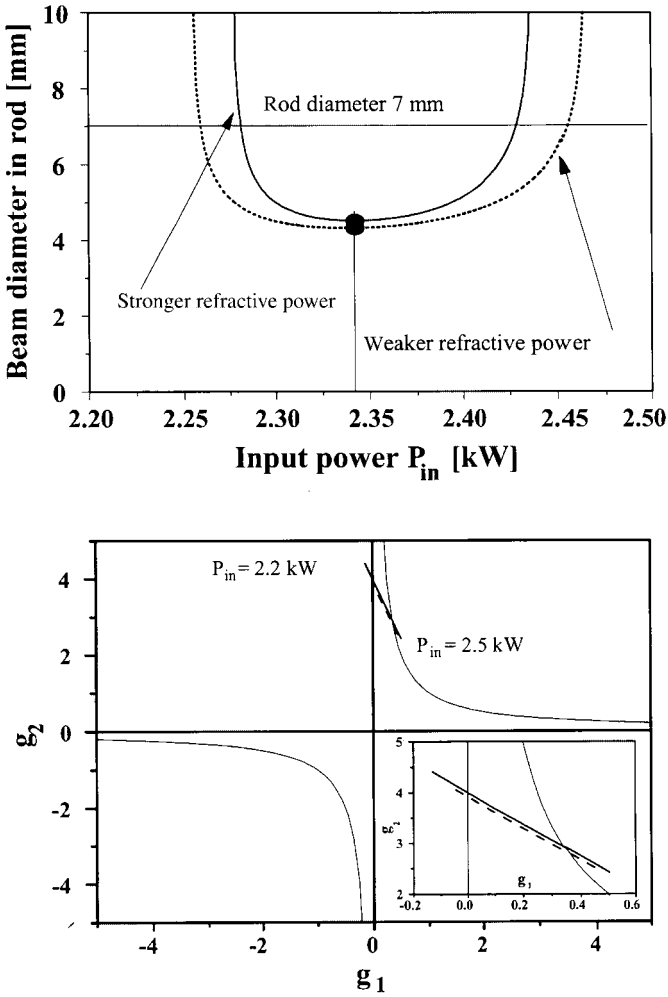

Figure 3.34. *Top:* Calculated stability ranges for the two dioptric powers of the Nd:YALO crystal in the start resonator. The resonator is designed for dynamically stable operation. Due to the compensation of the astigmatic thermal lens of the Nd:YALO, the stability ranges are centered to each other. *Bottom: g*-Diagram for the two dioptric powers. Both top and bottom are calculated for an optimal telescope length adjustment at $P_{in} = 2.34$ kW.

transverse fundamental mode diameter in the laser rod required for efficient operation leads to a longer resonator length.

3.7.2 Output data of the flashlamp-pumped SBS laser This laser was pumped by two flashlamps with a total electrical pulse energy of 100 J and a pump pulse duration of 1 ms. A maximum pump power of 3.2 kW was reached at the

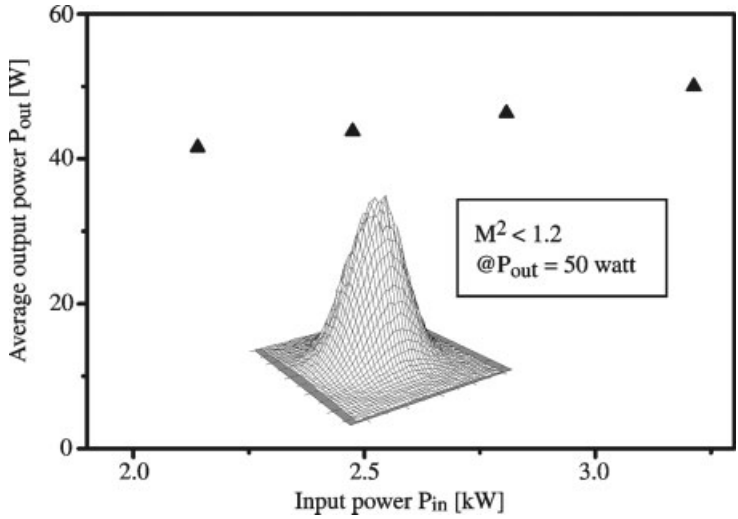

Figure 3.35. Average output power of SBS-laser oscillator as a function of pump power. Four measurements are shown with telescope lengths changed in steps of 3 cm. The depicted beam shape is measured at an average output power of 50 W of the SBS laser.

maximum repetition rate of 33 Hz. Using this laser head in a short multimode cavity, the total efficiency $\eta_{\text{tot}} = P_{\text{out}}/P_{\text{in}}$, the ratio of output to pump power, was $\eta_{\text{tot}} = 4.3\%$.

A maximum average output power of 50 W was achieved operating this SBS laser (see Fig. 3.35). It was reached with a telescope length of 32 cm at a pump power of 3.2 kW, which is equivalent to a total efficiency of 1.6%. At a pump power of 2.1 kW, an efficiency of 1.9% and an output power of 41 W was obtained. Unlike other *Q*-switch techniques, the SBS mirror is even able to enhance the efficiency of the free running laser because of its phase conjugating properties. The total efficiency of the same laser without the SBS mirror but with a 100% reflecting mirror M_{start} was measured to be 1.8% at a pump power of $P_{\text{in}} = 2.1$ kW. The maximum output power of this conventional free running laser without an SBS mirror was 43 W at a pump power of 2.7 kW. The beam quality was measured to be better than $M^2 < 1.2$. Within the measurement accuracy the beam qualities were the same for both the conventional and the SBS laser. As a result of the astigmatism of the Nd:YALO, the beam is slightly elliptical with a ratio of the two main axes of 1.1 at the highest output power.

During the pump pulse of duration of 1 ms, a burst of 22–16 *Q*-switch pulses related to the pump power range of 2–3.2 kW was emitted (see Fig. 3.36). In this pump power range the burst energy decreases from 2 J to 1.6 J. The *Q*-switch pulses within in the burst were separated by 40–53 μs. The single pulse energy was about 95 mJ. The *Q*-switch pulse duration was 60 ns (full width at half-maximum).

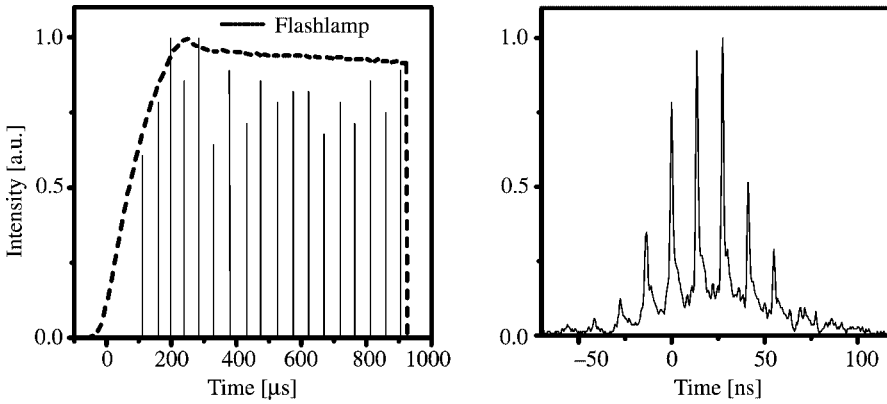

Figure 3.36. Temporal structure of the SBS-laser pulses. *Left:* Burst of *Q*-switch pulses of the SBS laser. *Right:* Single *Q*-switch pulse of the burst.

The strong modulation in the *Q*-switch pulse shown in Fig. 3.36 originates from the coupling of the longitudinal modes by the nonlinear SBS mirror (see Section 3.6.3). The basic period of the modulation is 13.7 ns and corresponds to an optical resonator length of 2.05 m. This is the length of the SBS resonator defined by the distance of mirror M1 and the focus in the SBS cell. For the high-power experiments presented in this section, no attempts were made to reach a certain pulse shape neither a strongly modulated nor a smooth pulse shape. The laser was optimized for a high average output power only. At the highest output power the stability of the burst energy fluctuated with a standard deviation of 10%. At an output power of 46 W the standard deviation is less than 5%.

In summary the efficiency of the SBS laser is even slightly higher than the efficiency of the corresponding laser with identical resonator but removed SBS mirror (to our knowledge there is no other fair comparison reported in the literature between an SBS- and equivalent conventional laser). Thus, the phase conjugating SBS mirror was confirmed to be a very efficient *Q*-switch device for higher pulse energies. Because the pinhole is designed for a high transmission of an undistorted TEM_{00} only, to a first approximation, aberrations of the TEM_{00} will not lead to a worse beam quality but will decrease the efficiency. The aberrations will be filtered out by the pinhole. But up to a pump power level of 2.7 kW the efficiency of the laser without the SBS mirror is only 0.1% smaller than the SBS laser.

Instead of the aberrations in the active material, it was found that the stability of the conventional start resonator is the limiting factor for the power scaling of the sf-SBS laser. At higher pump power levels the stability of the start resonator became more and more problematic. If a further increase in the average output power is desired, the fluctuating start resonator stability is the first problem that has to be solved by developing further advanced start resonator concepts.

3.7.3 Conclusion The realization of high-power SBS-laser oscillators leads to high-brightness lasers with a very efficient passive Q switch. So far the stability of the conventional start resonator limits the realized SBS-laser oscillators in their average output power. Phase conjugating MOPA systems do not have any stability problem because of their separation of low-power oscillator and high-power amplification. Either an improvement of the start resonator or a new concept for the entire SBS-laser oscillator is necessary to take full advantage of the promises of the theoretical analysis of SBS-PCRs. However, if single-frequency radiation is not required or may be even broad bandwidth desired, the SBS-laser oscillator is a simpler approach to realize a high-brightness laser compared to MOPA concepts for diffraction-limited beams up to a certain power level.

REFERENCES

1. B. Y. Zeldovich, V. I. Popovichev, V. V. Ragulskii, and F. S. Failzullov, Connection between the wave fronts of the reflected and exciting light in stimulated Mandelshtam–Brillouin scattering, *ZhETF Pis. Red.* **15**, 109–112 (1972).
2. G. C. Valley, A review of stimulated Brillouin scattering excited with a broad-band pump laser, *IEEE J. Quantum Electron.* **22**, 704–711 (1986).
3. R. A. Lamb and M. J. Damzen, Phase locking of multiple stimulated Brillouin scattering by a phase-conjugate laser resonator, *J. Opt. Soc. Am. B* **13**, 1468–1472 (1996).
4. M. J. Damzen, R. A. Lamb, and G. K. N. Wong, Ultrashort pulse generation by phase locking of multiple stimulated Brillouin scattering, *Opt. Commun.* **82**, 337–341 (1991).
5. B. Barrientos, V. Aboites, and M. Damzen, Temporal dynamics of a ring dye laser with a stimulated Brillouin scattering mirror, *Appl. Opt.* **35**, 5386–5391 (1996).
6. R. A. Lamb, Single longitudinal-mode, phase conjugating ring master oscillator power amplifier using external stimulated-Brillouin-scattering Q-switching, *J. Opt. Soc. Am. B* **13**, 1758 (1996).
7. S. Seidel, Improvement of extraction efficiency by regenerative amplification in an Nd-YAG-MOPA with a phase-conjugating SBS cell, *Opt. Quantum Electron.* **27**, 625–632 (1995).
8. A. D. Case, P. J. Soan, M. J. Damzen, and M. H. R. Hutchinson, *J. Opt. Soc. Am. B* **9**, 374 (1992).
9. A. D. Case, M. R. Osborne, M. J. Damzen, and M. H. R. Hutchinson, *Opt. Commun.* **69**, 311 (1989).
10. M. J. Damzen and H. R. Hutchinson, *Opt. Lett.* **5**, 282 (1984).
11. M. R. Osborne, W. A. Schroeder, M. J. Damzen, and H. R. Hutchinson, *Appl. Phys. B* **48**, 351 (1989).
12. S. A. Lesnik, M. S. Soskin, and A. I. Khizhnyak, Laser with a stimulated-Brillouin-scattering complex-conjugate mirror, *Sov. Phys. Tech. Phys.* **24,** 1249–1250 (1979).
13. I. Y. Anikeev, and J. Munch, Improved output power performance of a phase conjugated laser oscillator, *Opt. Quantum Electron* **31**, 545–553 (1999).
14. V. I. Odintsov and L. F. Rogacheva, *Pis'ma Zh. Eksp. Theor. Fiz.* **36**, 281 (1982).

15. G. K. N. Wong and M. J. Damzen, Enhancement of the phase conjugate stimulated Brillouin scattering process using optical feedback, *J. Mod. Opt.* **35**, 483 (1988).
16. G. K. N. Wong and M. J. Damzen, Investigations of optical feedback used to enhance stimulated scattering, *IEEE J. Quantum Electron.* **26**, 139 (1990).
17. K. D. Ridley, and A. M. Scott, Stimulated Brillouin scattering in a transverse resonator, *J. Opt. Soc. Am. B* **11**, 1361–1366 (1994).
18. A. M. Scott, and W. T. Whitney, Characteristics of a Brillouin ring resonator used for phase conjugation at 2.1 μm, *J. Opt. Soc. Am. B* **12**, 1634–1641 (1995).
19. H. Meng and H. J. Eichler, Nd:YAG laser with a phase-conjugating mirror based on stimulated Brillouin scattering in SF_6 gas, *Opt. Lett.* **16**, 569–571 (1991).
20. A. Kummrow, R. Menzel, D. Schumann, and H. J. Eichler, Length tuning effect in SBS-lasers, *Int. J. Nonlinear Opt. Phys.* **2**, 261–266 (1993).
21. J. Auyeng, D. Fekete, D. M. Pepper, and A. Yariv, A theoretical and experimental investigation of the modes of optical resonators with phase-conjugate mirrors, *IEEE J. Quantum Electron.* **15**, 1180–1188 (1979).
22. M. D. Skeldon and R. W. Boyd, Transverse-mode structure of a phase-conjugate oscillator based on Brillouin-enhanced four-wave mixing, *IEEE Quantum Electronics* **25**, 588–594, (1989)
23. A. M. Scott and K. D. Ridley, A review of Brillouin-enhanced-four-wave-mixing, *IEEE J. Quantum Electron.* **25**, 438–459 (1989).
24. D. Pohl, A new laser *Q*-switch-technique using stimulated Brillouin scattering **24A**, 239 (1967).
25. Y. Jingguo and J. Hongwei, Self-*Q*-switching Nd:YAG laser operation using stimulated thermal Rayleigh scattering, *Opt. Quantum Electron.* **26**, 929–932 (1994).
26. H. J. Eichler, S. Heinrich, and J. Schwartz, Self-starting short-pulse XeCl laser with a stimulated Brillouin scattering mirror, *Opt Lett.* **21**, 1909–1911 (1996).
27. M. Ostermeyer and R. Menzel, 50 Watt average output power with 1.2*DL beam quality from a single rod Nd:YALO laser with phase-conjugating SBS mirror, *Opt. Commun.* **171**, 85–91 (1999).
28. M. Ostermeyer, A. Heuer, and R. Menzel, 27 Watt average output power with 1.2*DL beam quality from a single rod Nd:YAG-laser with phase conjugating SBS-mirror, *IEEE J. Quantum Electron.* **34**, 372–377 (1998).
29. H. J. Eichler, R. Menzel, and D. Schumann, 10-W single rod Nd:YAG laser with stimulated Brillouin scattering *Q*-switching mirror, *Appl. Opt.* **31**, 5038–5043 (1992).
30. N. N. Il'ichev, A. A. Malyutin, and P. P. Pashinin, Laser with diffraction-limited divergence and *Q* switching by stimulated Brillouin scattering, *Sov. J. Quantum Electron.* **12**, 1161–1164 (1982).
31. I. Y. Anikeev and J. Munch, Variation in the coherence length of a phase conjugating oscillator, *Opt. Commun.* **178**, 449–456 (2000).
32. A. Drobnik and L. Wolf, Influence of self-focusing on the operation of a neodymium glass laser, *Sov. J. Quantum Electron.* **8**, 274–275 (1978).
33. V. I. Bezrodnyi, F. I. Ibragimov, V. I. Kislenko, R. A. Petrenko, V. L. Strrizhevskii, and E. A. Tikhonov, Mechanism of laser *Q* switching by intracavity stimulated scattering, *Sov. J. Quantum Electron.* **10**, 382–383 (1980).
34. A. Z. Grasyuk, V. V. Ragul'skii, and F. S. Faizullov, *JETP Lett.* **9**, 6 (1969).

35. A. Agnesi and G. C. Reali, Passive and self-*Q*-switching of phase-conjugation Nd:YAG laser oscillators, *Opt. Commun.* **89**, 41–46 (1992).

36. S. Chandra, R. C. Fukuda, and R. Utano, Sidearm stimulated scattering phase-conjugated laser resonator, *Opt. Lett.* **10**, 356–358 (1985).

37. M. R. Perrone and Y. B. Yao, Phase conjugated XECL laser resonator, *Opt. Lett.* **19**, 1052–1054 (1994).

38. P. P. Pashinin and E. J. Shklovsky, Laser with a stimulated Brillouin scattering mirror switched on by its own priming radiation, *Sov. J. Quantum Electron.* **18**, 1190 (1988).

39. B. I. Denker, I. Kertes, P. P. Pashinin, V. S. Sidorin, and E. J. Shklovsky, Compact laser with a stimulated Brillouin scattering mirror operated at pulse repetition frequency up to 150 Hz, *Sov. J. Quantum Electron.* **20**, 770 (1990).

40. S. Seidel and G. Phillipps, Pulse lengthening by intracavity stimulated Brillouin-scattering in a *Q*-switched, phase-conjugate Nd-YAG laser-oscillator, *Appl. Optics* **32**, 7408–7417 (1993).

41. A. B. Vasilev, O. M. Vokhnik, L. S. Korntsenko, V. A. Mikhailov, V. A. Spazkin, and I. A. Sherbakov, Lasing in apolarization-closed cavity with stimulated Brillouin scattering mirror, *Opt. Spektrosk.* **75**, 877–880 (1993).

42. O. M. Vokhnik, V. A. Mikhailov, V. A. Spahakin, I. V. Terent'eva, and I. A. Sherbakov, Solid state laser with a loop SBS-mirror, *Opt. Spektrosk.* **78**, 303 (1995).

43. P. P. Pashinin, E. J. Shklovsky, C. Y. Tang, and V. V. Tumorin, Passivly *Q*-switched single frequency Nd:YAG ring laser with feedback and phase conjugation, *Laser Phys.* **99**, 340 (1999).

44. B. Barrientos, V. Aboites, and M. J. Damzen, Temporal dynamics of an external-injection dye laser with a stimulated Brillouin scattering reflector, *J. Opt. (Paris)* **26**, 97–104 (1995).

45. M. J. Damzen, M. H. R. Hutchinson, and W. A. Schroeder, Single-frequency phase conjugate laser resonator using stimulated Brillouin scattering, *Opt. Lett.* **12**, 45 (1987).

46. W. A. Schroeder, M. J. Damzen, and M. H. R. Hutchinson, Studies of a single-frequency stimulated-Brillouin-scattering phase conjugate Nd:YAG laser oscillator, *J. Opt. Soc. Am. B* **6**, 171 (1989).

47. J. F. Lam and W. P. Brown, Optical resonators with phase conjugate mirrors, *Opt. Lett.* **5**, 61 (1980).

48. A. E. Siegman, P. A. Belanger, and A. Hardy, in *Optical Phase Conjugation*, R. A. Fischer (ed.), Academic Press, New York, (1983), Chapter 13, Optical Resonators Using Phase-Conjugate Mirrors.

49. P. A. Bélanger, A. Hardy, and A. E. Siegman, *Appl. Opt.* **19**, 602 (1980).

50. A. E. Siegmann, *Lasers*, Chapter 21, University Science Books, Mill Valley, California (1986).

51. G. Giuliani, M. Denariez-Roberge, and P. A. Belanger, Transverse modes of a stimulated scattering phase-conjugate resonator, *Appl. Opt.* **21**, 3719–3724, (1982).

52. G. G. Kochemasov and V. D. Nikolaev, Reproduction of the spatial amplitude and phase distributions of a pump beam in stimulated Brillouin scattering, *Sov. J. Quantum Electron.* **7**, 60–63 (1977).

53. P. A. Belanger and C. Paré, in *Optical Phase Conjugation*, M. Gower and D. Proch (eds.), Springer-Verlag, Berlin, (1994), Chapter 10, Phase Conjugate Resonators.

54. P. A. Belanger, A. Hardy, and A. E. Siegman, Resonant modes of optical cavities with phase-conjugate mirrors: Higher order modes, *Appl. Opt.* **19**, 479 (1980).
55. A. Hardy, Sensitivity of phase conjugate resonators to intracavity phase perturbations, *IEEE J. Quantum Electron.* **17**, 1581 (1981).
56. J. Schultheiss, Diploma thesis, University of Potsdam, 1996.
57. W. Koechner, *Solid State Laser Engineering*, 3rd ed., Springer-Verlag, (1992), Chapter 8.1.
58. M. Ostermeyer, K. Mittler, and R. Menzel, *Q* switch and longitudinal modes of a laser oscillator with a stimulated-Brillouin-scattering mirror, *Phys. Rev. A* **59**, 3975–3985 (1999).
59. M. J. Damzen, M. H. R. Hutchinson, and W. A. Schroeder, Direct measurements of the acoustic decay times of hypersonic waves generated by SBS, *IEEE J. Quantum Electron.* **23**, 328–334 (1987).
60. A. M. Scott, Brillouin induced four wave mixing, *Laser Wavefront Control, Proceedings of the SPIE*, Vol. 1000 (1988).
61. G. K. N. Wong and M. J. Damzen, Multiple Frequency Interaction in Stimulated Brillouin Scattering, Internal Report, The Blackett Laboratory, Imperial College, 1990.
62. A. Kummrow, R. Menzel, and D. Schumann, Resonant emission of a solid state laser with stimulated Brillouin scattering mirror, *J. Opt. Soc Am. B*, submitted.
63. P. Narum, M. D. Skeldon, and R. W. Boyd, Effect of laser mode structure on stimulated Brillouin scattering, *IEEE J. Quantum Electron.* **22**, 2161–2167 (1986).
64. N. Hodgson and H. Weber, *IEEE J. Quantum Electron.* **29**, 2497, (1993).
65. V. Magni, *J. Opt. Soc. Am. A* **4**, 1962 (1987).
66. R. Menzel, and M. Ostermeyer, Fundamental mode determination for guaranteeing diffraction limited beam quality of lasers with high output powers, *Opt Commun.* **149**, 321–325 (1998).
67. R. Menzel and H. J. Eichler, *Phys. Rev. A* **46**, 7139 (1992).
68. R. A. Mullen, *IEEE J. Quantum Electron.* **26**, 1299 (1990).